arXiv:1403.6777v1 [cond-mat.stat-mech] 26 Mar 2014

Equation of state for supercooled water at pressures up to 400 MPa

Vincent Holten, Jan V. Sengers, and Mikhail A. Anisimov[a)]

Institute for Physical Science and Technology and Department of Chemical and Biomolecular Engineering, University of Maryland, College Park, Maryland 20742, USA

(Dated: 28 March 2014)

An equation of state is presented for the thermodynamic properties of cold and supercooled water. It is valid for temperatures from the homogeneous ice nucleation temperature up to 300 K and for pressures up to 400 MPa, and can be extrapolated up to 1000 MPa. The equation of state is compared with experimental data for density, expansion coefficient, isothermal compressibility, speed of sound, and heat capacity. Estimates for the accuracy of the equation are given. The melting curve of ice I is calculated from the phase-equilibrium condition between the proposed equation and an existing equation of state for ice I.

Key words: compressibility; density; equation of state; expansivity; heat capacity; speed of sound; supercooled water; thermodynamic properties

Contents

1. Introduction 1

2. Experimental Data 2
2.1. Density 2
2.2. Density derivatives 2
2.3. Speed of sound 2
2.4. Heat capacity 4
2.5. Values from IAPWS-95 5
2.6. Adjustment of data 5
2.7. Values for extrapolation 6

3. Equation of State 6
3.1. Structure of the equation 6
3.2. Optimization method 8

4. Comparison with Experimental Data 9
4.1. Density 9
4.2. Expansivity 10
4.3. Isothermal compressibility 12
4.4. Speed of sound 13
4.5. Heat capacity 14
4.6. Extrapolation to 1000 MPa 15
4.7. Connection to IAPWS-95 16
4.8. Uncertainty estimates 16
4.9. Ice I melting curve 16

5. Conclusion 18

Acknowledgments 18

A. Homogeneous Nucleation Curve 18

B. Derivatives 19

C. Tables 19

References 19

[a)]Author to whom correspondence should be addressed; electronic mail: anisimov@umd.edu

1. Introduction

Supercooled water has been of interest to science since it was first described by Fahrenheit in 1724.[1] At atmospheric pressure, water can exist as a metastable liquid down to 235 K, and supercooled water has been observed in clouds down to this temperature.[2,3] Properties of supercooled water are important for meteorological and climate models[4,5] and for cryobiology.[6,7] Furthermore, the thermodynamic properties of cold and supercooled water at high pressure are needed for the design of food processing.[8]

It is well known that several properties of supercooled water – such as the isobaric heat capacity, the expansion coefficient, and the isothermal compressibility – show anomalous behavior; they increase or decrease rapidly with cooling. A liquid–liquid phase transition, terminated by a critical point, hidden below the homogeneous ice nucleation temperature has been proposed to explain this anomalous thermodynamic behavior.[9,10]

Several equations of state for supercooled water have been published. Sato[11] proposed an equation of state for water in the liquid phase including the metastable state, valid up to 100 MPa. Jeffery and Austin[12,13] developed an analytic equation of state of H_2O that also covers the supercooled region. Kiselev and Ely[14] made an early attempt to describe supercooled water in terms of an equation of state incorporating critical behavior. Anisimov and coworkers[15–18] also based their equations of state on an assumed liquid–liquid critical point. Since the publication of these equations, new experimental data have become available that enable development of an equation of state with a significantly improved accuracy.

The equation of state of this work was developed with the following aims:

1. It should represent the experimental data of liquid water

in the metastable region as well as possible. This work only considers supercooled water above the homogeneous nucleation temperature. The equation does not cover the glassy state of water (below 136 K at atmospheric pressure[19]).

2. It should be possible to smoothly connect this correlation to the IAPWS-95 formulation, the current reference for the thermodynamic properties of water.[20,21] IAPWS-95 is, strictly speaking, valid only at temperatures above the melting curve. When extrapolated into the supercooled region, the IAPWS-95 formulation also yields a good description of the data that were available at the time this formulation was developed. With a smooth connection, one could use IAPWS-95 at high temperatures and the present correlation at low temperatures, without significant discontinuities at the point of switching.

3. The correlation should allow extrapolation up to 1000 MPa. There are only a few data in the supercooled region above 400 MPa, but smooth extrapolation up to 1000 MPa would be desirable.

2. Experimental Data

Most of the experimental data that were considered in this work have been reviewed before.[17,20,22–25] In this section, we mainly discuss new data and data that were treated differently than in our previous work.[17,18,26]

2.1. Density

The experimental density data that were considered in this work are listed in Table I and shown in Fig. 1(a). Additional references to older data can be found in the articles of Tekáč *et al.*[50] and Wagner and Pruß.[20] In a large part of the supercooled region, the only available density data are those of Mishima.[38] As a result, it is difficult to estimate the systematic error of these data at low temperatures. In a graph in his article,[38] Mishima showed the random (type A) uncertainty for each data point, which is 0.2% on average and at most 0.5%. The systematic (type B) uncertainty can only be estimated above 253 K, in the region of overlap with density data of Kell and Whalley,[30] Sotani *et al.*,[35] and Asada *et al.*[37] In this region, the densities of Mishima deviate systematically by up to 0.4% from these other data. Below 253 K, the systematic uncertainty is unknown. As in earlier work,[17] we adjusted the density values of Mishima, under the assumption that the systematic deviation at low temperatures, where it is not known, is the same as at higher temperatures, where it can be calculated. It was found that the adjusted data of Mishima do not completely agree with the expansivity measurements of Ter Minassian *et al.*,[44] which we consider to be more accurate. Therefore, the adjusted data of Mishima were included in the fit of the equation of state with a relatively low weight.

The only experimental density data at atmospheric pressure that were included in the fit are those of Hare and Sorensen,[34] which are considered to be the best available. For pressures higher than atmospheric, we included data from Sotani *et al.*,[35] Asada *et al.*,[37] and Kell and Whalley.[30] To enable extrapolation of the equation above 400 MPa, density data from Grindley and Lind[28] up to 800 MPa were included in the fit.

2.2. Density derivatives

Several data sets exist for temperature and pressure derivatives of the density ρ. The cubic expansion coefficient α_P, also known as expansivity, is defined as

$$\alpha_P = -\frac{1}{\rho}\left(\frac{\partial\rho}{\partial T}\right)_P, \tag{1}$$

where T is the temperature and P is the pressure. The isothermal compressibility κ_T is defined as

$$\kappa_T = \frac{1}{\rho}\left(\frac{\partial\rho}{\partial P}\right)_T. \tag{2}$$

The data sets listed in Table II were all included in the fit, with the exception of the compressibility data of Mishima.[38] Mishima's data were not included because they may be affected by systematic errors of unknown size at low temperatures. In previous work,[17,18] expansivities reported by Hare and Sorensen[34] were included in the fit. However, Hare and Sorensen did not measure the expansivity directly, but derived it from a fit to their density data. Because we already included Hare and Sorensen's density data in our fit, their expansivity data were not used in the fit. Expansivity values from Ter Minassian *et al.*[44] were calculated from their empirical correlation. The accuracy of their correlation is not given; the relative difference with expansivities calculated from IAPWS-95 is at most 3.2% in the range of 300 K to 380 K and 0 MPa to 400 MPa.

At points in the phase diagram where the expansivity is zero, the density has a maximum with respect to temperature. The temperature at which this occurs is usually referred to as the temperature of maximum density (TMD). Caldwell[45] measured the TMD for pressures up to 38 MPa, and these measurements were included in the expansivity data set of the fit as $\alpha_P = 0$ points. The recent TMD measurements of Hiro *et al.*[51] were not used, because they deviate systematically by about 1.5 K from more accurate data.

2.3. Speed of sound

The experimental data on the speed of sound considered in this article are given in Table III and shown in Fig. 2. Recent data that were not considered in previous work are the accurate measurements of the speed of sound by Lin and Trusler[52] down to of 253 K and from 1 MPa to 400 MPa. Although there are few data points in the supercooled region, the accuracy of 0.03%–0.04% makes this an important data set. Lin and Trusler also derived densities and isobaric heat capacities by integrating their speed-of-sound data. We have not considered these derived properties in the development of the equation of state in this work for the following reason. To enable integration of the speed of sound, Lin and Trusler represented their experimental data on the speed of sound by an empirical correlation. The experimental data of Lin and Trusler are closer

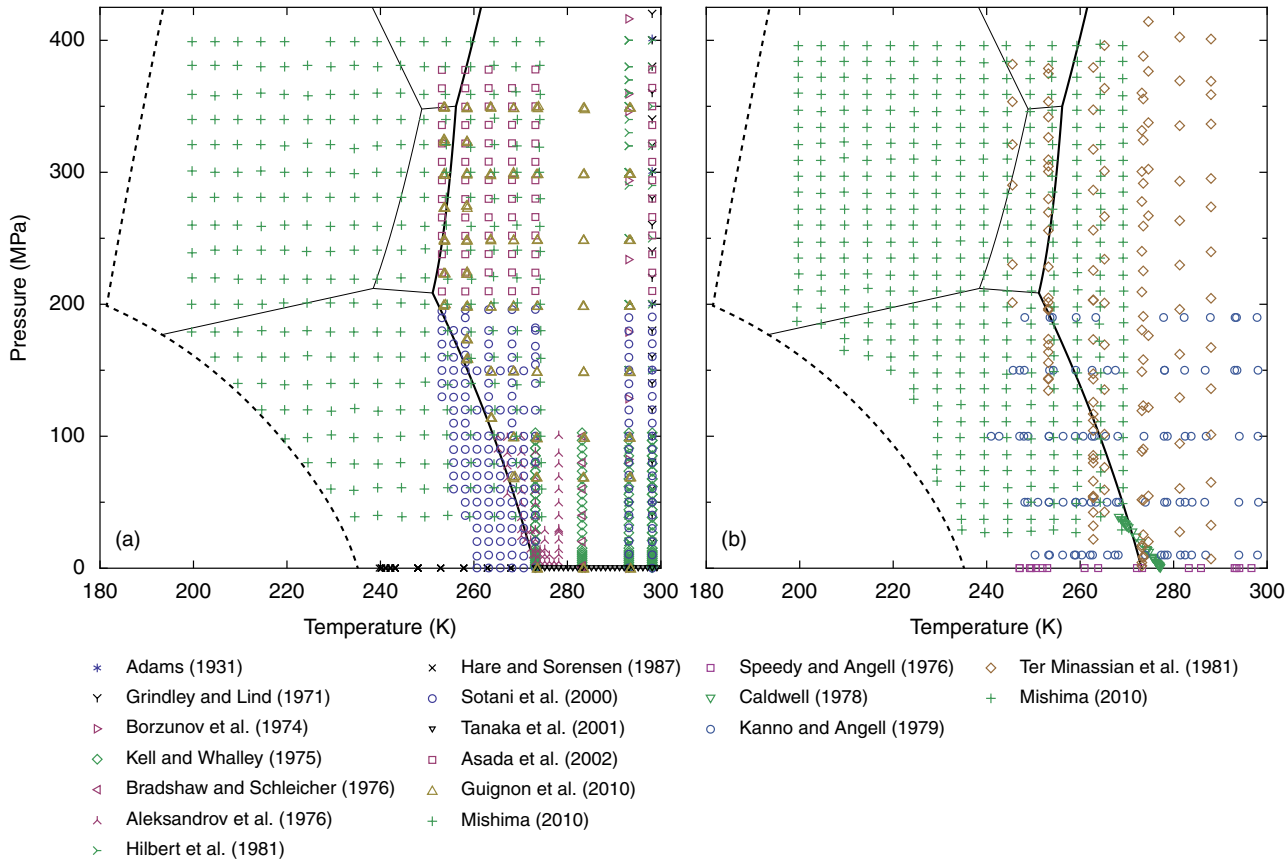

FIG. 1. (a) Location of experimental H_2O density data considered in this work.[27–39] The thick solid curve is the melting curve,[40,41] the dashed curve is the homogeneous ice nucleation limit (see Appendix A), and the thin solid curves are the ice phase boundaries.[42,43] (b) Location of the experimental H_2O density-derivative data. Ter Minassian *et al.*[44] and Caldwell[45] have measured the expansivity; other authors[38,46,47] have measured the isothermal compressibility.

TABLE I. Experimental density data

Reference	Year	Temperature range (K)	Pressure range (MPa)	Density uncertainty (%)	Source[a]	Included in fit
Adams[27]	1931	298	0.1–900	0.1	T	–
Grindley & Lind[28]	1971	298–423	20–800	0.02	T	Yes
Borzunov *et al.*[29]	1974	293–338	0–923	0.1	T	–
Kell & Whalley[30]	1975	273–423	0.5–103	0.001–0.003	T	Yes
Bradshaw & Schleicher[31]	1976	283	0.1–100	0.007	T	–
Aleksandrov *et al.*[32]	1976	264–278	5–101	0.1[c]	T	–
Hare & Sorensen[34]	1987	240–268	0.101325	0.02	T	Yes
Sotani *et al.*[48]	1998	253–293	0–200	0.05	–[b]	–
Sotani *et al.*[35]	2000	253–298	0–196	0.03[c]	G	Yes
Tanaka *et al.*[36]	2001	273–313	0.101325	0.0001	T	–
Asada *et al.*[37]	2002	253–298	210–378	0.1	G	Yes
Guignon *et al.*[39]	2010	254–323	0.1–350	0.2	T	–
Mishima[38]	2010	200–275	39–399	0.5[d]	S	Yes

[a] T = table from article, S = table from supplement, G = extracted from graph
[b] Superseded by Sotani *et al.*[35]
[c] Estimated by Wagner and Thol[49]
[d] Uncertainty is unknown below 253 K, see the text

TABLE II. Experimental data on compressibility and expansivity

Reference	Year	Temperature range (K)	Pressure range (MPa)	Source[a]
Compressibility data				
Speedy & Angell[46]	1976	247–297	0.101325	G
Kanno & Angell[47]	1979	241–298	10–190	G
Mishima[38]	2010	199–269	27–397	S
Expansivity data				
Caldwell[45]	1978	268–277	0.1–38	T[b]
Ter Minassian *et al.*[44]	1981	246–410	2–636	G[b]

[a] T = table from article, S = table from supplement, G = extracted from graph
[b] An empirical correlation is also provided

to the prediction of our equation of state than to their correlation, in the temperature range considered here (Sec. 4.4) Therefore, densities and heat capacities calculated from our equation of state are more accurate than the values derived by Lin and Trusler.

The work of Smith and Lawson[53] deserves mention because they were likely the first to measure the speed of sound below 273 K at elevated pressures. However, their pressure calibration has an uncertainty of about 1%, as discussed by Holton *et al.*,[54] and their data were not further considered for this work.

The most accurate measurements of the speed of sound in the range from 273 K to 300 K and up to 60 MPa are those of Belogol'skii *et al.*[55] They presented a correlation that represents their data with a standard deviation of 0.003% in the speed of sound. We estimated the accuracy of this correlation by comparing it to the experimental data of Lin and Trusler. For this comparison, Lin and Trusler's speeds of sound on each of their isotherms were corrected to compensate for their small deviation at atmospheric pressure. After this correction, the difference between the data of Lin and Trusler and the correlation of Belogol'skii *et al.* is at most 0.01%, which suggests that the correlation of Belogol'skii *et al.* has an accuracy of 0.01% or better in the speed of sound. Measurements of Aleksandrov and Larkin[56] in this temperature and pressure range have a slightly higher uncertainty of 0.02%. The data presented by Mamedov[57] are not considered here, because Mamedov published rounded data of Aleksandrov and Larkin.[56] Aleksandrov and Kochetov[58] used the setup described by Aleksandrov and Larkin[56] to measure the speed of sound down to 266 K and up to 100 MPa. A comparison with the data of Lin and Trusler[52] suggests that the accuracy of the data of Aleksandrov and Kochetov[58] is about 0.1%.

To improve the extrapolation behavior of the equation above 400 MPa, data from Vance and Brown[59] up to 700 MPa were included in the fit. The data from Hidalgo Baltasar *et al.*,[60] which also extend up to 700 MPa, were not included because they systematically deviate from other data (Sec. 4.4)

At atmospheric pressure in the supercooled region, the data of Taschin *et al.*[61] seem to be the best available; they are consistent with other thermodynamic properties.[61] Above 273.15 K, the data deviate at most 0.15% from the IAPWS-95 formulation, and the uncertainty below 260 K is 0.7%.

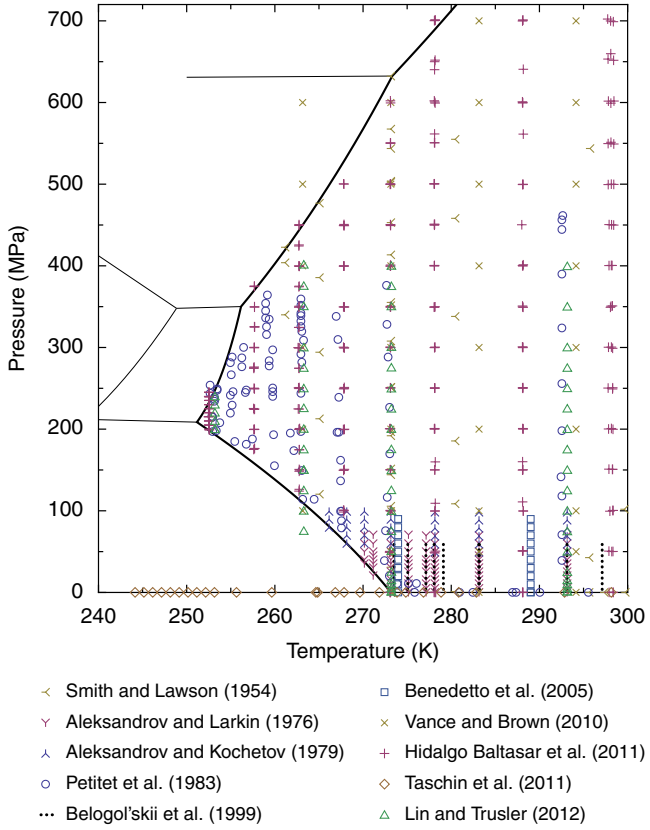

FIG. 2. Location of experimental data on the speed of sound considered in this work.[52,53,55,56,58–61,68,69] The thick curve is the melting curve,[40,41] and the thin curves are the ice phase boundaries.[42,43] Belogol'skii *et al.*[55] did not publish their individual data points; their reported isotherms are shown as dotted lines.

2.4. Heat capacity

The isobaric heat capacity C_P of cold and supercooled water at atmospheric pressure has been measured by several investigators; a list is given in Table IV. There are two data sets that extend down to 236 K, those of Angell *et al.*[71] and Archer and Carter.[72] The difference between the data sets increases with decreasing temperature, and at 236 K, the heat capacity reported by Angell *et al.*[71] is 5% higher than that found by Archer and Carter.[72] Because it is not known which data set is best, the equation of the current work was initially not fitted to any heat-capacity data in the supercooled region. It was found that most of the preliminary equations predicted heat capacities in agreement with the data of Angell *et al.*,[71] and were close to values calculated from the extrapolated IAPWS-95 formulation. However, in some cases, the predicted heat capacities were slightly higher than those Angell *et al.*[71] Therefore, to reduce the difference with the experimental data, values calculated from IAPWS-95 were added as input for the fit.

There are only few measurements of C_P at elevated pressures. The data of Sirota *et al.*[73] at pressures up to 98 MPa were included in the fit. The data of Czarnota[74] were not considered accurate enough to be included in the fit.

TABLE III. Experimental data on the speed of sound

Reference	Year	Temperature range (K)	Pressure range (MPa)	Frequency (MHz)	Speed-of-sound uncertainty (%)	Source[a]	Included in fit
Smith & Lawson[53]	1954	261–402	0.1–923	12	–	T	–
Wilson[62]	1959	274–364	0.1–97	5	0.1[b]	T	–
Del Grosso & Mader[63]	1972	273–368	0.101325	5	0.001	T	–
Aleksandrov & Larkin[56]	1976	270–647	0.1–71	3	0.02[c]	T	Yes
Trinh & Apfel[64,65]	1978	256–283	0.101325	2–3	0.2	G	–
Aleksandrov & Kochetov[58]	1979	266–423	6–99	2.5, 5.6	0.1	T	–
Bacri & Rajaonarison[66]	1979	247–280	0.101325	925	–	G	–
Trinh & Apfel[67]	1980	240–256	0.101325	0.054	1.3	G	–
Petitet *et al.*[68]	1983	253–296	0.1–462	10	0.1	T	–
Belogol'skii *et al.*[55]	1999	273–313	0.1–60	5–10	0.01[d]	C	Yes
Benedetto *et al.*[69]	2005	274–394	0.1–90	5	0.05	T	–
Vance & Brown[59]	2010	263–371	0.1–700	400–700	0.2–0.3	T	Yes
Taschin *et al.*[61,70]	2011	244–363	0.101325	140	0.7	A	Yes
Hidalgo Baltasar *et al.*[60]	2011	252–350	0.1–705	2	0.2–0.3	T	–
Lin & Trusler[52]	2012	253–473	1–401	5	0.03–0.04	T	Yes

[a] T = table from article, A = data provided by authors, G = extracted from graph, C = calculated from correlation
[b] Wilson[62] estimated the uncertainty at 0.01%. The estimate of 0.1% is from Sato *et al.*[24]
[c] Uncertainty below 303 K, estimated from comparison with values from Belogol'skii *et al.*[55]
[d] Estimated from comparison with data from Lin & Trusler[52] after correcting for systematic deviations at atmospheric pressure

TABLE IV. Experimental heat-capacity data

Reference	Year	Temperature range (K)	Pressure [a] range (MPa)	Source[b]
Osborne *et al.*[76]	1939	274–368		T
Sirota *et al.*[73]	1970	272–306	20–98	T
Anisimov *et al.*[77]	1972	266–304		G
Angell *et al.*[78]	1973	235–273		T[c]
Angell *et al.*[71]	1982	236–290		T
Czarnota[74]	1984	299–300	224–1032	T
Bertolini *et al.*[79]	1985	247–254		G
Tombari *et al.*[80]	1999	245–283		A
Archer & Carter[81]	2000	236–285		T

[a] Data are at 0.101325 MPa unless otherwise specified
[b] T = table from article, A = data provided by authors, G = extracted from graph
[c] Superseded by Angell *et al.*[71]

Recently, Manyà *et al.*[75] have measured C_P at 4 MPa from 298 K to 465 K. The results of Manyà *et al.* imply that the derivative $(\partial C_P/\partial P)_T$ is positive for pressures lower than 4 MPa, which contradicts the thermodynamic relation $(\partial C_P/\partial P)_T = -T(\partial^2 V/\partial T^2)_P$, where V is the specific volume. Hence, the data of Manyà *et al.* were not considered in this work.

2.5. Values from IAPWS-95

To ensure a smooth connection to the IAPWS-95 formulation, the equation of state from this work was fitted to property values calculated from IAPWS-95 in the temperature and pressure range defined by

$$T/\mathrm{K} \geq 273.15 + (P/\mathrm{MPa} - 0.1)/12, \quad 300 \leq T/\mathrm{K} \leq 325. \tag{3}$$

This range, shown in Fig. 3, was determined from the differences between values calculated from IAPWS-95 and from preliminary fits, as well as the deviations from experimental data. Within the range defined by Eq. (3), only IAPWS-95 values were included in the final fit. In addition, the equation of state was also fitted to values from IAPWS-95 at atmospheric pressure from 273.15 K to 300 K. The locations of all data that were included in the fit are shown in Fig. 3.

2.6. Adjustment of data

Temperatures in this work are expressed on the international temperature scale of 1990 (ITS-90).[82] Temperatures on the IPTS-68 scale were converted to ITS-90 according to the equation of Rusby.[83] Temperatures on the IPTS-48 scale were first converted to IPTS-68 and then to ITS-90. The conversion from IPTS-48 to IPTS-68 was performed according to the equations given by Bedford and Kirby;[84] these conversion equations were found to agree with those of Douglas.[85] In the temperature range considered in this work, the ITS-27 and IPTS-48 scales can be considered as identical,[86] so temperatures on the ITS-27 scale were treated as IPTS-48 temperatures. In principle, the values of quantities that depend on temperature intervals, such as the expansion coefficient and the heat capacity, should also be converted.[72,83,87] In this work, such an adjustment was only found to be necessary for the accurate heat-capacity measurements at atmospheric pressure close to the melting temperature;[76,77] the changes in heat capacity due to the conversion were less than 0.1%.

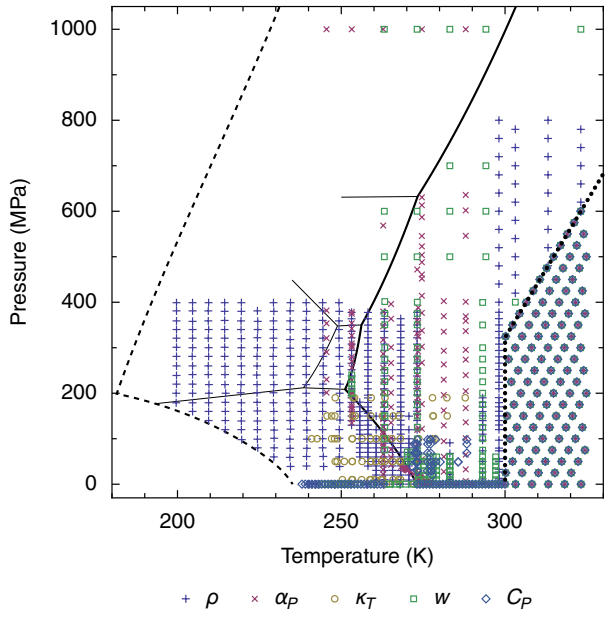

FIG. 3. Location of the experimental data on density ρ, thermal expansivity α_P, isothermal compressibility κ_T, speed of sound w, and isobaric heat capacity C_P that were selected as input for the fit. On the dotted line and to the right of it, the source of the data is the IAPWS-95 formulation. The thick solid curve is the melting curve,[40,41] the dashed curve is the homogeneous ice nucleation limit (see Appendix A), and the thin solid curves are the ice phase boundaries.[42,43]

The absolute volumes measured by Bradshaw and Schleicher[31] were converted to densities, where the mass of the samples was calculated from the IAPWS-95 value for the density at atmospheric pressure. The density data of Grindley and Lind[28] show a slight systematic deviation from more accurate data.[20] To prevent this deviation from affecting the fit, the data from Grindley and Lind were corrected for this deviation. In the figures in this article, the data of Grindley and Lind are shown without this adjustment. The speed of sound measurements of Lin and Trusler[52] at 273.21 K show a small systematic deviation from more accurate data,[55,63] and speed-of-sound values on this isotherm were increased by 0.025% to compensate for this deviation. In the figures, the original values of Lin and Trusler[52] are shown.

Many data for supercooled water are available only in graphical form and have not been published as numerical values. In the case of recent publications, we requested the authors to provide us with data in tabular form. In the case of older data or when the authors could not be reached, the data were extracted from graphs. For all references, the data source that we used is indicated in the tables in this section. All data are provided in tabular form in the supplemental material.[88]

2.7. Values for extrapolation

To enable extrapolation of the equation of state to 1000 MPa, it was found necessary to guide the fit at high pressures by including estimated values for the expansivity and speed of sound at 1000 MPa (Fig. 3).

3. Equation of State

3.1. Structure of the equation

The thermodynamic formulation presented here is a mean-field version of an equation of state developed in Ref. 18. It is based on the so-called two-state model, in which it is assumed that liquid water is a mixture of a high-density structure A and a low-density structure B. There is experimental evidence for the existence of two distinct local structures in water.[89,90]

Competition between these structures naturally explains the density anomaly and other thermodynamic anomalies in cold water. In particular, if the excess Gibbs energy of mixing of these two structures is positive, the nonideality of the "mixture" can be sufficient to cause liquid–liquid separation, or, at least, to significantly reduce the stability of the homogeneous liquid phase and consequently generate the anomalies in the thermodynamic response functions. However, since experimental data are not yet available beyond the homogeneous ice nucleation limit, the possibility of a liquid–liquid transition in water must be postulated and is to be examined by indirect means. The location of the hypothesized liquid–liquid critical point, characterized by the critical temperature T_c and critical pressure P_c, is obtained from the extrapolation of the properties far away from the transition, thus making it very uncertain.[17,18]

We introduce the dimensionless quantities

$$\hat{T} = \frac{T}{T_c}, \qquad \hat{P} = \frac{PV_0}{RT_c}, \qquad \hat{G} = \frac{G}{RT_c}, \qquad \hat{V} = \frac{V}{V_0}, \tag{4}$$

$$\hat{S} = \frac{S}{R}, \qquad t = \frac{T-T_c}{T_c}, \qquad p = \frac{(P-P_c)V_0}{RT_c}, \tag{5}$$

where T is the temperature, P is the pressure, G is the specific Gibbs energy, R is the specific gas constant, V is the specific volume, V_0 is a reference volume, and S is the specific entropy. We adopt the equation of state for the Gibbs energy in the form of "athermal mixing", suggested in Ref. 16 and 18,

$$\hat{G} = \hat{G}^{\mathrm{A}} + \hat{T}\left[xL + x\ln x + (1-x)\ln(1-x) + \omega x(1-x)\right], \tag{6}$$

where $\hat{G}^{\mathrm{A}}$ is the Gibbs energy of the high-density structure, x is the fraction of the low-density structure, ω is an interaction parameter, and

$$L = \frac{\hat{G}^{\mathrm{B}} - \hat{G}^{\mathrm{A}}}{\hat{T}}, \tag{7}$$

with $\hat{G}^{\mathrm{B}}$ the Gibbs energy of the low-density structure. The difference in Gibbs energy between the pure components $\hat{G}^{\mathrm{B}} - \hat{G}^{\mathrm{A}}$ is related to the equilibrium constant K of the "reaction" $A \rightleftharpoons B$,

$$\ln K \equiv L. \tag{8}$$

For the interaction parameter ω in Eq. (6), a linear pressure dependence is taken,

$$\omega = 2 + \omega_0 p. \tag{9}$$

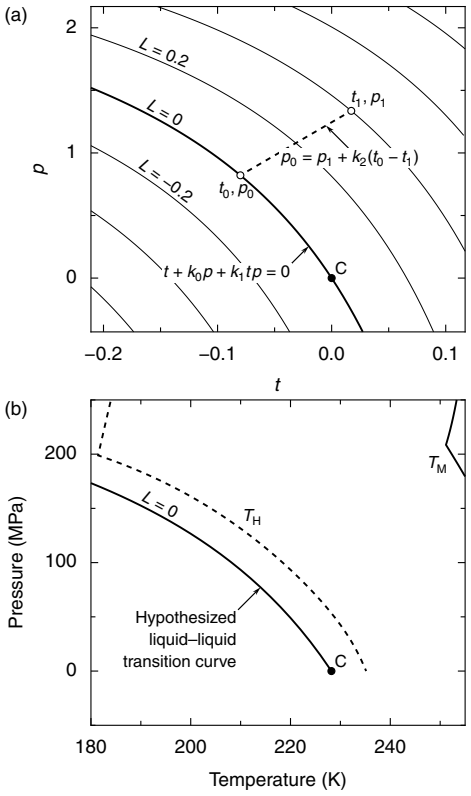

FIG. 4. (a) Construction of the field L. Solid curves are contour lines of constant L, with the $L = 0$ contour, defined by Eq. (10), drawn thicker. The point (t_1, p_1) is projected on the $L = 0$ curve along the dashed line with slope $\mathrm{d}p/\mathrm{d}t = k_2$, given by Eq. (12), yielding the point (t_0, p_0). The field L is taken proportional to the distance between the two points. The critical point is indicated by C. All contour lines have the same shape, but are shifted in the p–t plane in the direction of the dashed line. (b) Predicted location of the low-density/high-density phase transition in the phase diagram. The curves labeled T_M and T_H represent the experimental melting temperature and temperature of homogeneous ice nucleation, respectively.

A low-density/high-density phase-transition curve is located at $L = 0$, for $\omega > 2$, and the phase separation occurs upon increase of pressure. This phase transition lies below the homogeneous ice nucleation temperature and cannot be observed in experiments. Experiments by Mishima[38,91] suggest that the phase transition curve, if it exists, lies close to the homogeneous nucleation curve, and has the same shape. In this work, we use a hyperbola for the $L = 0$ phase-transition curve, as in previous work,[17,18]

$$t + k_0 p + k_1 t p = 0, \tag{10}$$

where k_0 is the slope $\mathrm{d}t/\mathrm{d}p$ of the $L = 0$ curve at the critical point, and k_1 determines the curvature. In this work, the expression for $L(t, p)$ is constructed as proportional to the distance to the $L = 0$ curve in the p–t diagram [Fig. 4(a)]. Consider a point in the phase diagram with dimensionless coordinates (t, p). The projection (t_0, p_0) of this point on the $L = 0$ curve, along a line with slope $\mathrm{d}p/\mathrm{d}t = k_2$, is found by the solution of the equations

$$t_0 + k_0 p_0 + k_1 t_0 p_0 = 0, \tag{11}$$
$$p_0 = p + k_2(t_0 - t), \tag{12}$$

which are illustrated in Fig. 4(a). The field L is taken proportional to the distance between the points (t, p) and (t_0, p_0) with proportionality factor L_0, which results in

$$L = L_0 \frac{K_2}{2k_1 k_2}\left[1 + k_0 k_2 + k_1(p + k_2 t) - K_1\right]. \tag{13}$$

with

$$K_1 = \left\{\left[1 + k_0 k_2 + k_1(p - k_2 t)\right]^2 - 4k_0 k_1 k_2 (p - k_2 t)\right\}^{1/2},$$
$$K_2 = (1 + k_2^2)^{1/2}. \tag{14}$$

The expression for L in Eq. (13) yields $L = 0$ if Eq. (10) is satisfied, as can be verified by solving for p in Eq. (10) and substituting the result in Eqs. (13) and (14). In previous work,[17,18] the simpler expression

$$L = L_0(t + k_0 p + k_1 t p) \tag{15}$$

was used, which yields the same location [Eq. (10)] for the $L = 0$ curve. Equation (15) is not valid for large L, corresponding to large pressures (about 1000 MPa at 310 K), where this equation generates an additional, unphysical root.

At any pressure and temperature, the equilibrium value x_e of the fraction x is found from the condition

$$\left(\frac{\partial G}{\partial x}\right)_{T,P} = 0 \quad \text{at} \quad x = x_\mathrm{e}, \tag{16}$$

which yields

$$L + \ln\frac{x_\mathrm{e}}{1 - x_\mathrm{e}} + \omega(1 - 2x_\mathrm{e}) = 0. \tag{17}$$

This equation must be solved numerically for the fraction x_e. The location of the critical point is defined by

$$\left(\frac{\partial^2 G}{\partial x^2}\right)_{T,P} = 0, \qquad \left(\frac{\partial^3 G}{\partial x^3}\right)_{T,P} = 0. \tag{18}$$

In the theory of critical thermodynamic behavior, the thermodynamic properties are expressed in terms of the order parameter and the ordering field. In our equation of state, L is the ordering field, and the order parameter ϕ is given by[92]

$$\phi = 2x_\mathrm{e} - 1. \tag{19}$$

The susceptibility χ defines the liquid–liquid stability limit (spinodal) as

$$\chi^{-1} = \frac{1}{2\hat{T}}\left(\frac{\partial^2 \hat{G}}{\partial x^2}\right)_{T,P} = 0, \tag{20}$$

and is given by

$$\chi = \left(\frac{2}{1 - \phi^2} - \omega\right)^{-1}. \tag{21}$$

The dimensionless volume and entropy can then be written as

$$\hat{V} = \frac{\hat{T}}{2}\left[\frac{\omega_0}{2}(1-\phi^2) + L_{\hat{P}}(\phi+1)\right] + \hat{G}^{\mathrm{A}}_{\hat{P}}, \tag{22}$$

$$\hat{S} = -\frac{\hat{T}L_{\hat{T}}}{2}(\phi+1) - \frac{\hat{G}-\hat{G}^{\mathrm{A}}}{\hat{T}} - \hat{G}^{\mathrm{A}}_{\hat{T}}, \tag{23}$$

with subscripts $\hat{T}$ and $\hat{P}$ indicating partial derivatives with respect to the subscripted quantity. Expressions for the derivatives of the field L and the Gibbs energy $\hat{G}^{\mathrm{A}}$ are given in Appendix B.

The dimensionless response functions, namely isothermal compressibility $\hat{\kappa}_T$, expansion coefficient $\hat{\alpha}_P$, and isobaric heat capacity $\hat{C}_P$, are given by

$$\hat{\kappa}_T = \frac{1}{\hat{V}}\left\{\frac{\hat{T}}{2}\left[\chi(L_{\hat{P}} - \omega_0\phi)^2 - (\phi+1)L_{\hat{P}\hat{P}}\right] - \hat{G}^{\mathrm{A}}_{\hat{P}\hat{P}}\right\}, \tag{24}$$

$$\hat{\alpha}_P = \frac{1}{\hat{V}}\left\{\frac{L_{\hat{T}\hat{P}}}{2}\hat{T}(\phi+1) + \frac{1}{2}\left[\frac{\omega_0}{2}(1-\phi^2) + L_{\hat{P}}(\phi+1)\right] - \frac{\hat{T}L_{\hat{T}}}{2}\chi(L_{\hat{P}} - \omega_0\phi) + \hat{G}^{\mathrm{A}}_{\hat{T}\hat{P}}\right\}, \tag{25}$$

$$\hat{C}_P = -L_{\hat{T}}\hat{T}(\phi+1) + \frac{\hat{T}^2}{2}\left[L^2_{\hat{T}}\chi - L_{\hat{T}\hat{T}}(\phi+1)\right] - \hat{T}\hat{G}^{\mathrm{A}}_{\hat{T}\hat{T}}. \tag{26}$$

These dimensionless quantities are defined as

$$\rho = \frac{\rho_0}{\hat{V}}, \quad \kappa_T = \frac{\hat{\kappa}_T}{\rho_0 R T_{\mathrm{c}}}, \quad \alpha_P = \frac{\hat{\alpha}_P}{T_{\mathrm{c}}}, \quad C_P = R\hat{C}_P, \tag{27}$$

with the density $\rho = 1/V$, $\rho_0 = 1/V_0$, and C_P the specific isobaric heat capacity. The specific isochoric heat capacity C_V is found from the thermodynamic relation

$$C_V = C_P - \frac{T\alpha_P^2}{\rho\kappa_T}, \tag{28}$$

and the speed of sound w is found from

$$w = \left(\rho\kappa_T\frac{C_V}{C_P}\right)^{-1/2} = \left(\rho\kappa_T - \frac{T\alpha_P^2}{C_P}\right)^{-1/2}. \tag{29}$$

Equation (6) is a mean-field equation of state which neglects effects of fluctuations.[92] In particular, not taking these effects into account results in a lower critical pressure,[18] see Table VI in Appendix C. As shown earlier,[17,26] a mean-field equation describes the experimental data for supercooled water equally well as a nonanalytic equation based on critical scaling theory. The reason for the good description by a mean-field approximation is that the region asymptotically close to the hidden critical point, where scaling theory would be necessary, is not experimentally accessible [Fig. 4(b)]. Moreover, in practice, a mean-field equation of state is more convenient for computational use than one incorporating scaling theory.

The Gibbs energy of the high-density structure $\hat{G}^{\mathrm{A}}$ is a function of dimensionless temperature and pressure τ and π, and serves as a background function in the two-state model. We selected the empirical form

$$\hat{G}^{\mathrm{A}}(\tau,\pi) = \sum_{i=1}^{n} c_i \tau^{a_i}\pi^{b_i}\mathrm{e}^{-d_i\pi}, \tag{30}$$

where n is the number of terms and a_i, b_i, c_i, and d_i are adjustable parameters. In previous work,[18] the exponents a_i and b_i were integers, and the dimensionless temperature and pressure were defined as $\tau = t$ and $\pi = p$. In this work, this definition could not be used, because t and p become negative below the critical point and powers of negative numbers with real exponents are generally complex numbers. To avoid negative τ and π, they were redefined as

$$\tau = \hat{T} = \frac{T}{T_{\mathrm{c}}}, \qquad \pi = \frac{(P-P_0)V_0}{RT_{\mathrm{c}}}, \tag{31}$$

where the offset $P_0 = -300$ MPa was chosen to enable extrapolation to negative pressures.

3.2. Optimization method

The aim of the least-squares optimization used in this work was to obtain a fit that minimizes χ^2, the sum of squared deviations of the fit from experimental data. To make these deviations dimensionless, the differences of experimental and calculated values were divided by the experimental uncertainty. The fit of Eq. (6) requires optimization of the parameters L_0, ρ_0, ω_0, and k_2 as well as the parameters a_i, b_i, c_i, and d_i for the Gibbs energy $\hat{G}^{\mathrm{A}}$ in Eq. (30). The optimization was carried out in two steps, and is roughly based on the procedure of Lemmon.[93] In the first step, a bank of 135 terms of the form

$$\tau^{a_i}\pi^{b_i}\mathrm{e}^{-d_i\pi} \tag{32}$$

was created, where the exponents a_i and b_i were restricted to integers in the range of 0 to 8, with $a_i + b_i \leq 8$. The coefficient d_i was restricted to the values 0, 0.6, and 1. The aim of the first optimization step was to find a good selection of 20 to 25 terms out of the 135 terms for the Gibbs energy $\hat{G}^{\mathrm{A}}$. Initially, $\hat{G}^{\mathrm{A}}$ contained a few manually selected terms with low values of the exponents a_i and b_i. The algorithm then determined the best term to add to $\hat{G}^{\mathrm{A}}$, in the following way. The first term in the bank of terms that was not in the selection was added, and all parameters except a_i, b_i, and d_i were optimized. The newly added term was then removed, another term was added, and the parameters were optimized again. This procedure was repeated for all terms and a value of χ^2 was computed for the addition of each term. The term that resulted in the lowest χ^2 was then permanently added to $\hat{G}^{\mathrm{A}}$. By repeating the addition procedure, the number of terms in $\hat{G}^{\mathrm{A}}$ was increased to about 20. The quality was then further improved by deleting terms that could be deleted without significantly increasing χ^2, and adding new terms to replace the deleted terms.

In the second optimization step, the parameters a_i, b_i, and d_i were also taken adjustable and optimized simultaneously with the other parameters. The additional degrees of freedom made it possible to delete terms while still improving the fit. Terms with similar values of the exponents were combined if that was possible without deteriorating the fit.

The shape of the liquid–liquid phase transition curve, the $L = 0$ curve of Eq. (10), was not taken adjustable. The parameters that determine this curve, k_0 and k_1 in Eq. (10), were derived from the shape of the experimental homogeneous nucleation curve, described in Appendix A. The initial location

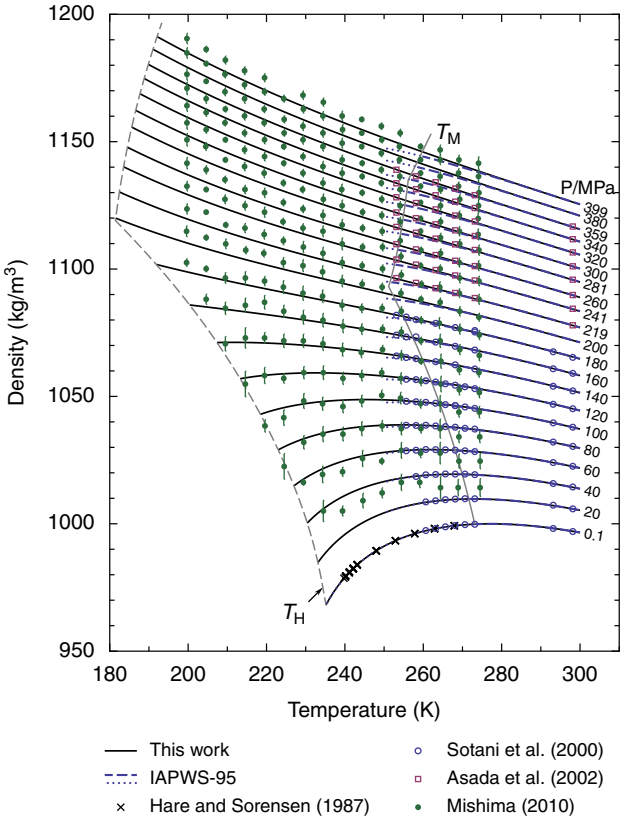

FIG. 5. Density of liquid water as a function of temperature and pressure. Solid black curves are calculated from Eq. (6), and symbols represent experimental data.[34,35,37,38] Vertical lines through the points of Mishima represent reported random uncertainties, and do not take systematic errors into account. T_M indicates the melting temperature and T_H the homogeneous nucleation temperature. In this figure, the densities of Asada *et al.*[37] are interpolated values that match the isobar pressures of Mishima.[38] Values calculated from IAPWS-95 are shown for comparison; dashed in the stable region and dotted in the metastable region.

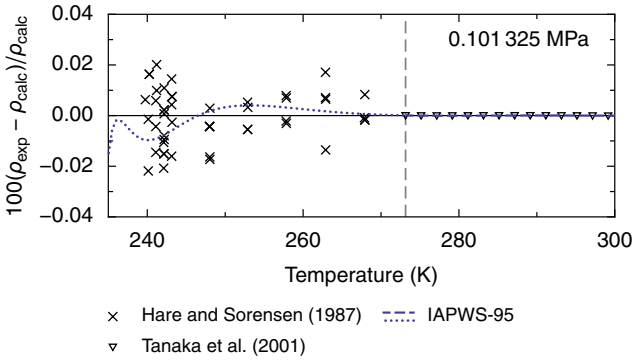

FIG. 6. Percentage deviations of experimental density data[34,36] at atmospheric pressure from values calculated from Eq. (6). Values calculated from IAPWS-95 are shown for comparison, dashed in the stable-liquid region and dotted in the metastable region. The vertical dashed line indicates the melting temperature.

of the liquid–liquid critical point was taken from the mean-field equation of state by Holten *et al.*[18] and was later adjusted to a slightly lower temperature to improve the description of experimental data. The numerical values of all parameters are listed in Appendix C, and computer code for the equation of state is included in the supplemental material.[88]

4. Comparison with Experimental Data

4.1. Density

In Fig. 5, the density calculated from Eq. (6) is plotted as a function of temperature for several isobars, and compared with experimental data. Below 250 K, Mishima's data are the only data that are available. As described in Sec. 2.1, Eq. (6) was fitted to these data with a low weight. The equation reproduces the trend of Mishima's data, and most of these densities are reproduced by Eq. (6) to within 0.5%. A comparison of Mishima's data with the more accurate data of Sotani *et al.*[35] and Asada *et al.*[37] shows that Mishima's data are systematically too low at low pressures and too high at high pressures, with deviations of up to 0.4%. The calculated density isobars in Fig. 5 below 150 MPa curve down at low temperature, while the isobars at higher pressures slightly curve upwards, and an inflection point is present for isobars above a certain pressure. This inflection is related to a minimum in the expansivity, as will be discussed in Sec. 4.2. For comparison purposes, figures in this section also include values calculated from the extrapolated IAPWS-95 formulation, down to 235 K at atmospheric pressure and down to 250 K at higher pressures.

In Fig. 6, experimental density values at atmospheric pressure are compared with values calculated from Eq. (6). Both Eq. (6) and the extrapolated IAPWS-95 formulation represent the data of Hare and Sorensen within the experimental scatter of about 0.02%. In the stable region, Eq. (6) differs less than 0.0001% (1 part per million) from the densities recommended by Tanaka *et al.*[36]

Figure 7 shows differences between experimental densities up to 400 MPa and values calculated from Eq. (6). The proposed equation represents the data of Sotani *et al.*[35] to within 0.02%, which is within the uncertainty of those data of 0.03% as estimated by Wagner and Thol.[49] The data of Asada *et al.*,[37] with an uncertainty of 0.1%, are reproduced to within 0.04%. The data of Guignon *et al.*[39] are represented to within the uncertainty of 0.2%. The density data of Grindley and Lind[28] deviate systematically from other data, as was noted by Wagner and Pruß.[20] At 298 K, IAPWS-95 agrees well with Eq. (6) and with the densities of Sotani *et al.*[35] and Asada *et al.*,[37] which were not available when IAPWS-95 was developed. The density data of Aleksandrov *et al.*[32] at temperatures above 271 K are in satisfactory agreement with the proposed equation of state. For example, at 273.15 K, the densities of Aleksandrov *et al.* differ less than 0.01% from the values calculated from Eq. (6). However, at lower temperatures, such as at 267 K and 270 K, their data show systematic deviations of up to 0.07% from the data of Sotani *et al.*[35] and, hence, from the proposed equation.

In the stable region up to 100 MPa, there are accurate density measurements of Kell and Whalley,[30] with an uncertainty

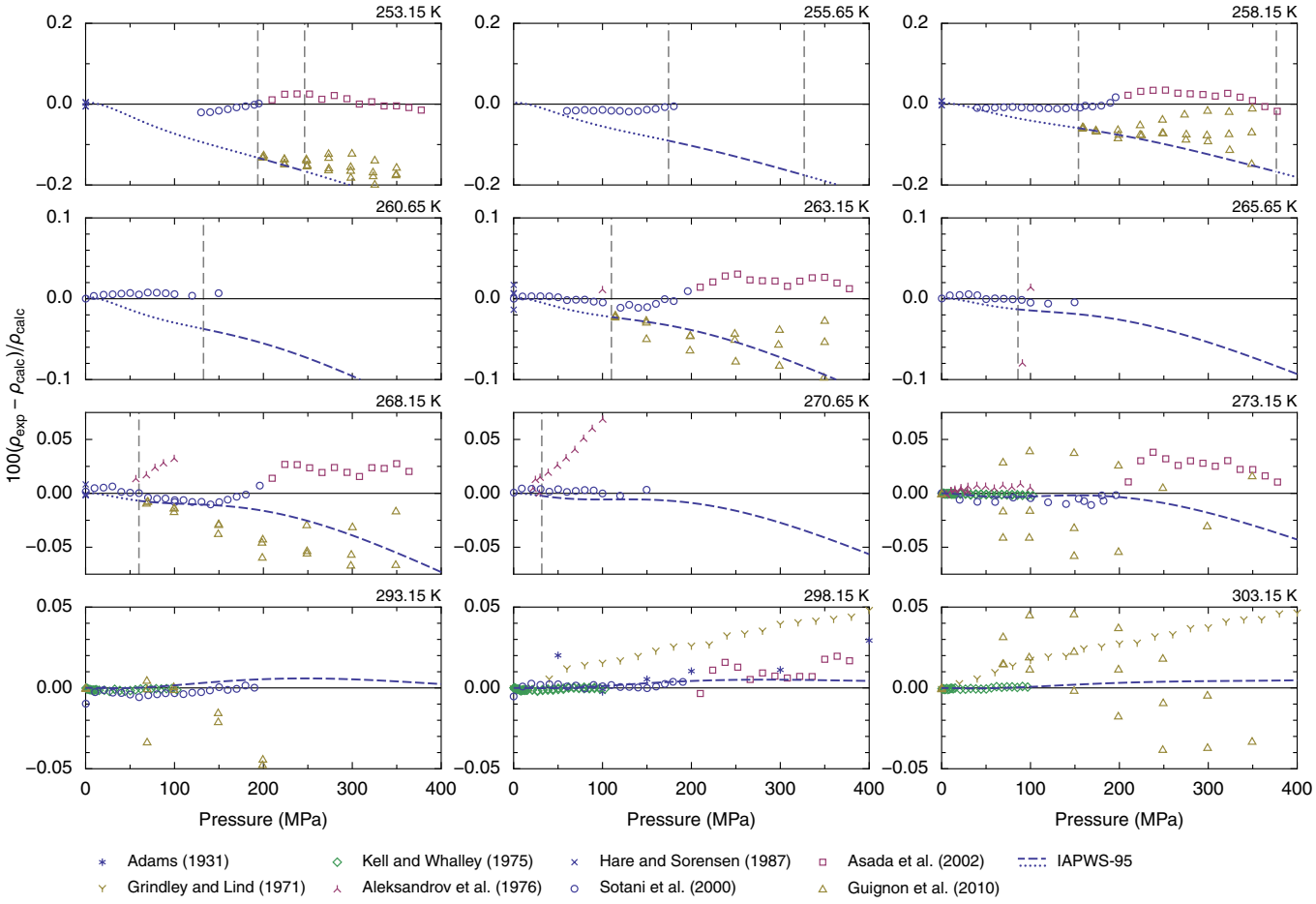

FIG. 7. Percentage deviations of experimental density data[27,28,30,34,35,37,39] from values calculated from Eq. (6). Values calculated from IAPWS-95 are plotted for comparison; dashed in the stable-liquid region and dotted in the metastable region. The vertical dashed lines indicate the melting pressure.

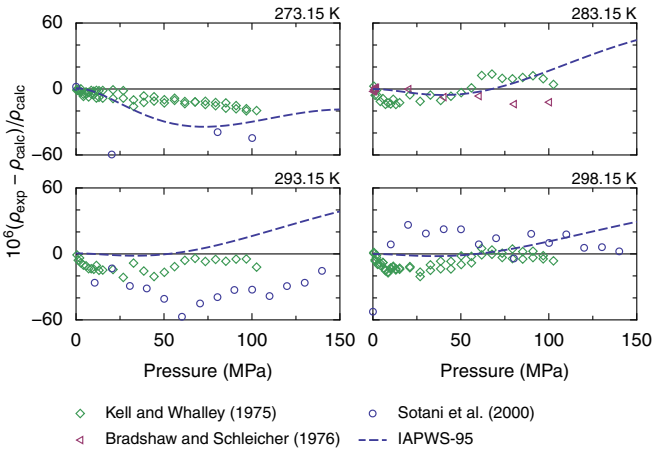

FIG. 8. Parts-per-million differences between experimental density data[30,31,35] and values calculated from Eq. (6). Values calculated from IAPWS-95 are plotted for comparison.

of 10 parts per million (ppm) at low pressures and 30 ppm at 100 MPa. Figure 8 shows that Eq. (6) represents these density data to within this uncertainty. Kell and Whalley adjusted their density data to bring them in agreement with the speed-of-sound data of Wilson,[62] which were the best available at the time. Figure 18, to be discussed in Sec. 4.4, shows that the speeds of sound of Wilson deviate up to 0.08% from more accurate data at 273 K. This deviation may be the reason for the small systematic deviation of the density data of Kell and Whalley from Eq. (6) at 273 K, seen in Fig. 8.

4.2. Expansivity

The expansivity calculated from Eq. (6) is compared with values calculated from the correlation of Ter Minassian *et al.*[44] and IAPWS-95 in Fig. 9. At atmospheric pressure, there is little difference in the expansivity values of Eq. (6) and the extrapolated IAPWS-95 formulation down to 250 K. At higher pressures, Eq. (6) follows the correlation of Ter Minassian *et al.*, to which it was fitted. More detailed deviations of the data of Ter Minassian *et al.* from Eq. (6) are shown in Fig. 10. These deviation plots use absolute instead of relative differences, because the expansivity passes through zero in the temperature and pressure range considered. Equation (6) represents the correlation of Ter Minassian *et al.* and most of their data points to within 2×10^{-5} K^{-1}.

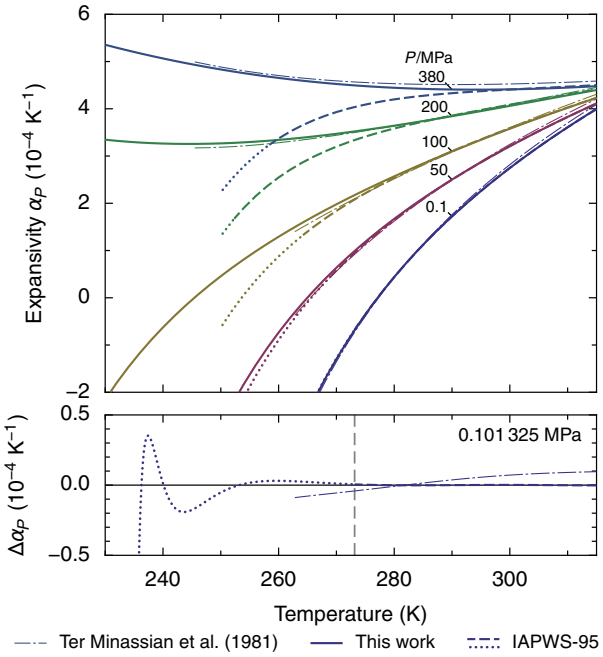

FIG. 9. Expansivity calculated from Eq. (6), the correlation of Ter Minassian *et al.*,[44] and IAPWS-95 (dashed in the stable-liquid region and dotted in the metastable region). The bottom panel shows the expansivity difference at atmospheric pressure, where values from Eq. (6) have been subtracted from values from IAPWS-95 and the correlation of Ter Minassian *et al.*[44] The vertical dashed line indicates the melting temperature.

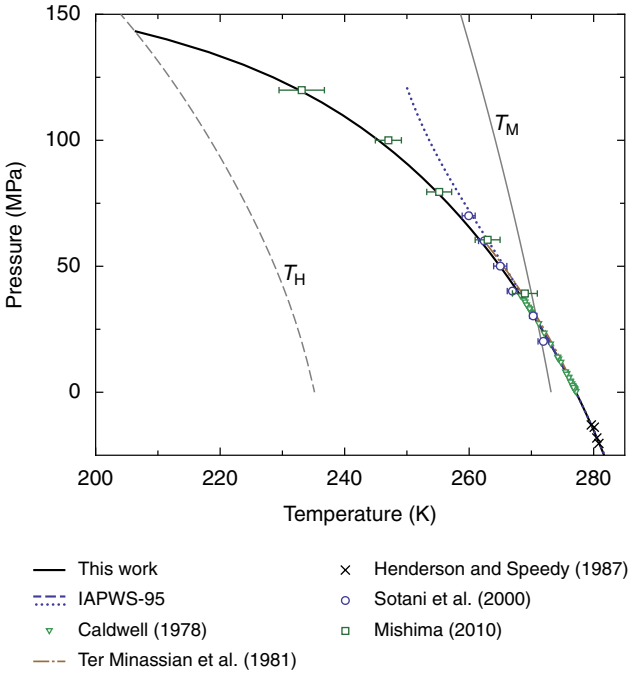

FIG. 11. Temperature of maximum density (TMD) and locus of zero expansivity, calculated from Eq. (6), the correlation of Ter Minassian *et al.*,[44] and IAPWS-95 (dashed in the stable-liquid region and dotted in the metastable region). Caldwell[45] and Henderson & Speedy[94] reported the TMD itself; the TMD of the data of Mishima[38] and Sotani *et al.*[35] was calculated from polynomial fits to their density data. The melting temperature and temperature of homogeneous nucleation are indicated by T_M and T_H, respectively.

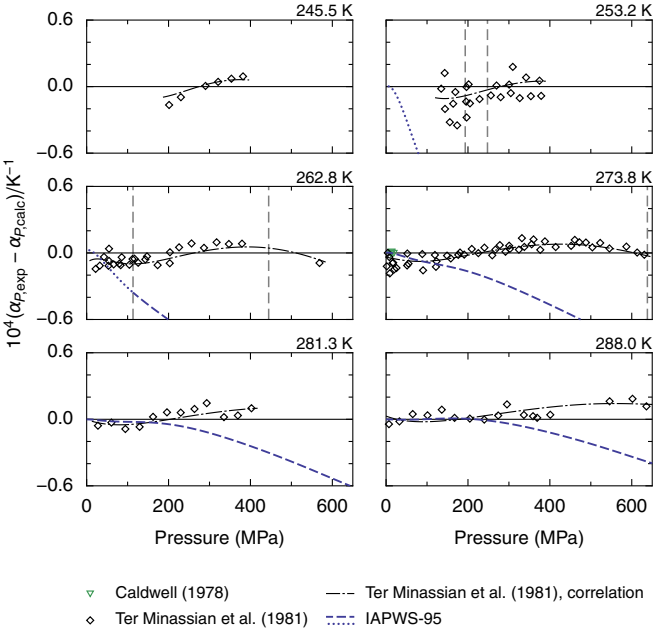

FIG. 10. Deviations of experimental expansivity data[44,45] from values calculated from Eq. (6). Vertical dashed lines indicate the melting pressure. Values calculated from IAPWS-95 are shown for comparison, dashed in the stable-liquid region and dotted in the metastable region. The correlation that Ter Minassian *et al.*[44] fitted to their data is also shown.

Experimental and calculated values for the temperature of maximum density (TMD) are shown in Fig. 11. The TMD moves to lower temperatures with increasing pressure, and the rate at which it does so also increases with pressure. The TMD corresponding to Mishima's data is relatively uncertain because of the scatter in his density data. Deviations of the experimental TMD values from Eq. (6) are plotted in Fig. 12. The data of Caldwell[45] are represented to within 0.08 K. The uncertainty δT in the TMD values calculated from the expansivity correlation of Ter Minassian *et al.*[44] can be estimated as

$$\delta T \approx \left| \left(\frac{\partial \alpha_P}{\partial T} \right)_P \right|^{-1} \delta \alpha_P, \tag{33}$$

where the temperature derivative of the expansivity is calculated from the correlation of Ter Minassian *et al.*[44] With an expansivity uncertainty $\delta\alpha_P$ of at least 10^{-5} K^{-1} (estimated from Fig. 10), Eq. (33) gives an uncertainty δT of 0.6 K at 0 MPa, increasing to 0.8 K at 60 MPa. When one takes these uncertainties into account, the correlation of Ter Minassian *et al.*[44] is consistent with the data of Caldwell[45] and with Eq. (6). The data of Henderson and Speedy[94] are represented fairly well by both Eq. (6) and IAPWS-95, when these equations are extrapolated to negative pressure.

The existence of a minimum in the expansivity,

$$\left(\frac{\partial \alpha_P}{\partial T} \right)_P = 0, \tag{34}$$

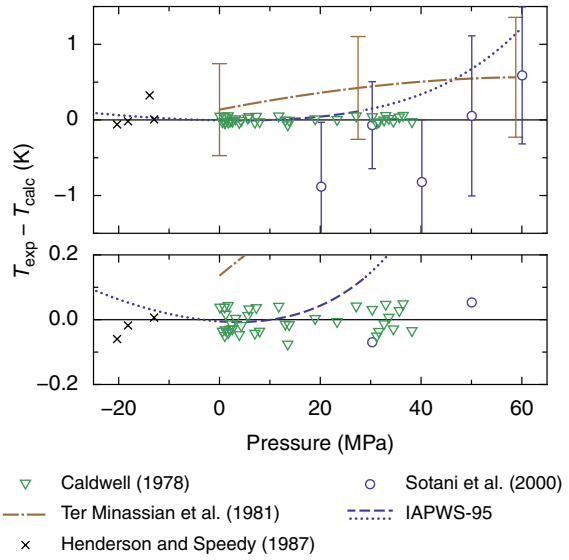

FIG. 12. Differences between experimental temperatures of maximum density[45,94] and values calculated from Eq. (6). Values calculated from density data of Sotani *et al.*,[35] the correlation of Ter Minassian *et al.*,[44] and IAPWS-95 (dashed in the stable-liquid region and dotted in the metastable region) are shown for comparison. The error bars on the curve of Ter Minassian *et al.*[44] represent the temperature uncertainty, derived from the uncertainty of their expansivity.

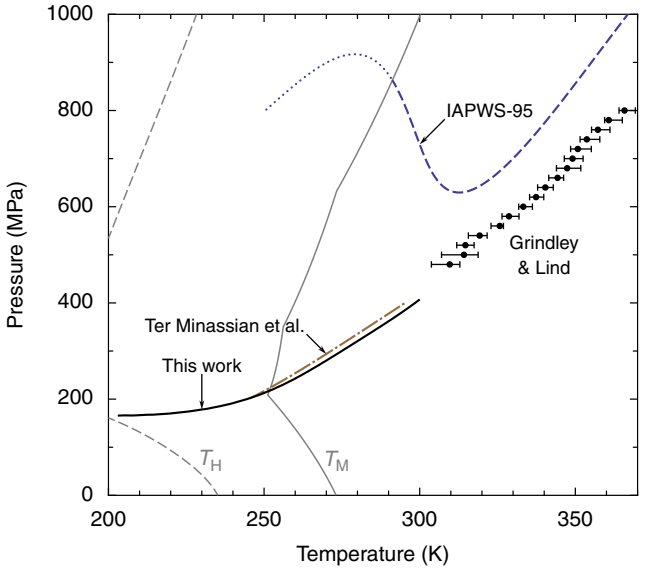

FIG. 13. Location at which the temperature derivative of the expansivity $(\partial\alpha_P/\partial T)_P$ is zero, for the correlation from this work, the data of Grindley and Lind,[28] the correlation of Ter Minassian *et al.*,[44] and the IAPWS-95 formulation. These locations represent minima of the expansivity, except for IAPWS-95 between 280 K and 310 K, where the extremum is a maximum. Values from IAPWS-95 are shown dotted in the region where IAPWS-95 was extrapolated. T_H and T_M indicate the homogenous nucleation temperature and the melting temperature, respectively.

was noticed by Ter Minassian *et al.*[44] and by Mishima[38] for temperatures lower than 300 K. The minimum in the expansivity is related to the inflection points in curves of the density versus temperature, as is visible in Fig. 5 above 200 MPa. The minimum is seen in the expansivity correlation of Ter Minassian *et al.*[44] in Fig. 9. An expansivity minimum is also present in the expansivity derived from the volume data of Grindley and Lind,[28] as shown in Fig. 13. We obtained the location of the expansivity minimum in the data of Grindley and Lind by fitting several polynomials of different order to all their volume data, and also to data on each isobar separately. For every isobar, this results in several estimated temperatures of the expansivity minimum. The differences in these temperatures were used to estimate the uncertainty of the minimum. The locus of expansivity minima of Grindley and Lind thus obtained can be smoothly connected to that of Ter Minassian *et al.*[44] Our equation of state closely follows the expansivity minimum obtained by Ter Minassian *et al.*,[44] as seen in Fig. 13.

4.3. Isothermal compressibility

Experimental data on the isothermal compressibility are shown in Fig. 14 together with values calculated from Eq. (6) and IAPWS-95. The data of Mishima[38] exhibit more scatter than those of Angell and coworkers,[46,47] but they show a consistent trend of a decrease in the anomalous behavior of the compressibility with increasing pressure. Deviations of the experimental data from Eq. (6) are plotted in Fig. 15. It can be seen in Fig. 15 that Eq. (6) represents the compressibility data of Speedy and Angell[46] and Kanno and Angell[47] to

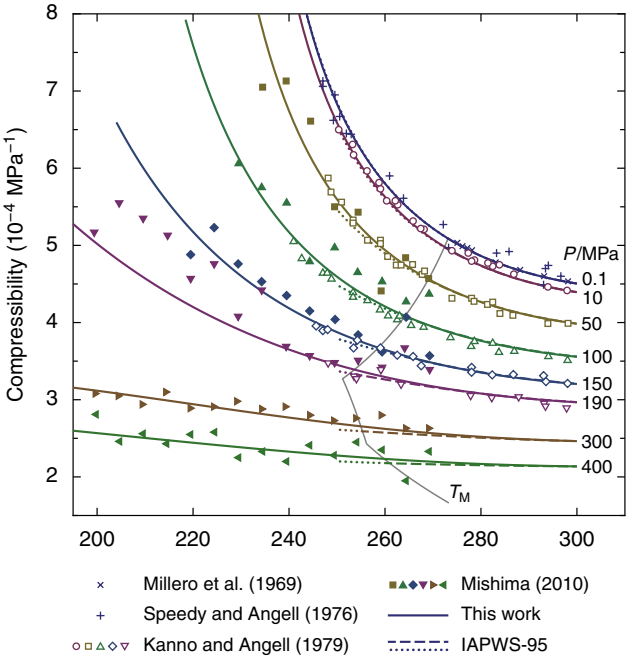

FIG. 14. Isothermal compressibility calculated from Eq. (6) (solid curves) and IAPWS-95 (dashed in the stable-liquid region and dotted in the metastable region). Symbols represent experimental data.[38,46,47,95] Solid and open symbols with the same shape belong to the same isobar. The curve marked T_M represents the melting temperature.

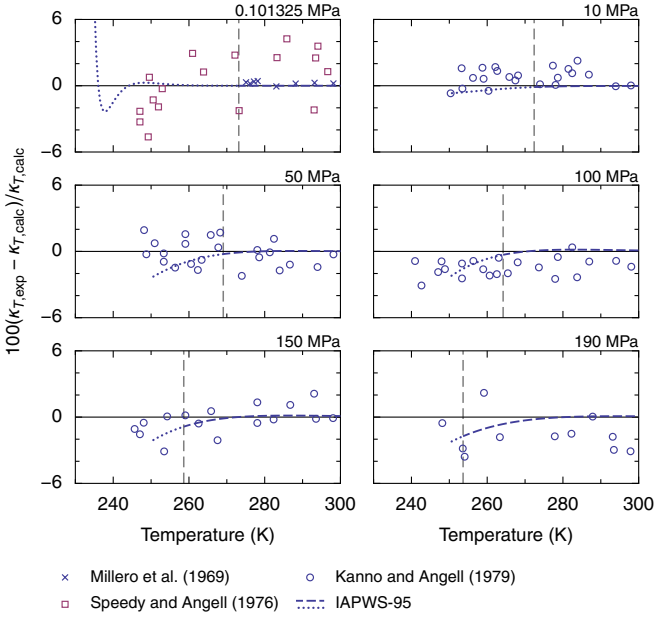

FIG. 15. Percentage deviations of experimental isothermal-compressibility data of Millero *et al.*,[95] Speedy and Angell,[46] and Kanno and Angell[47] from values calculated from Eq. (6). Values from IAPWS-95 are shown for comparison (dashed in the stable-liquid region and dotted in the metastable region). Dashed vertical lines represent melting temperatures.

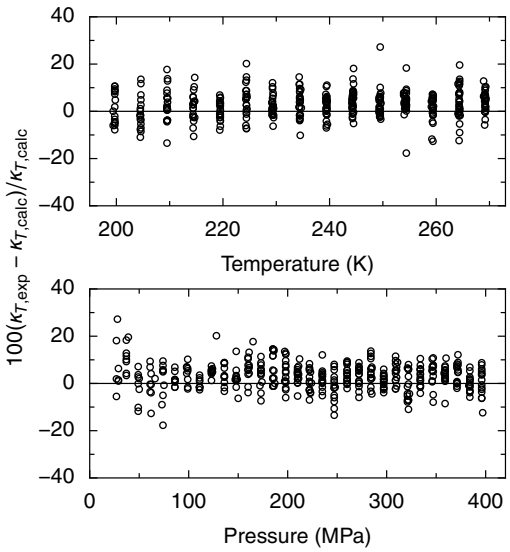

FIG. 16. Percentage deviations of experimental isothermal-compressibility data of Mishima[38] from values calculated from Eq. (6), as a function of temperature and pressure.

within their scatter. The difference between the extrapolated IAPWS-95 formulation and Eq. (6) increases with decreasing temperature; this difference is related to the density difference between the two equations shown in Fig. 5. The deviation of the compressibilities measured by Mishima[38] from Eq. (6) is shown in Fig. 16. Although Eq. (6) was not fitted to Mishima's compressibility data, it represents them fairly well when one takes into account the experimental scatter of about ±10%.

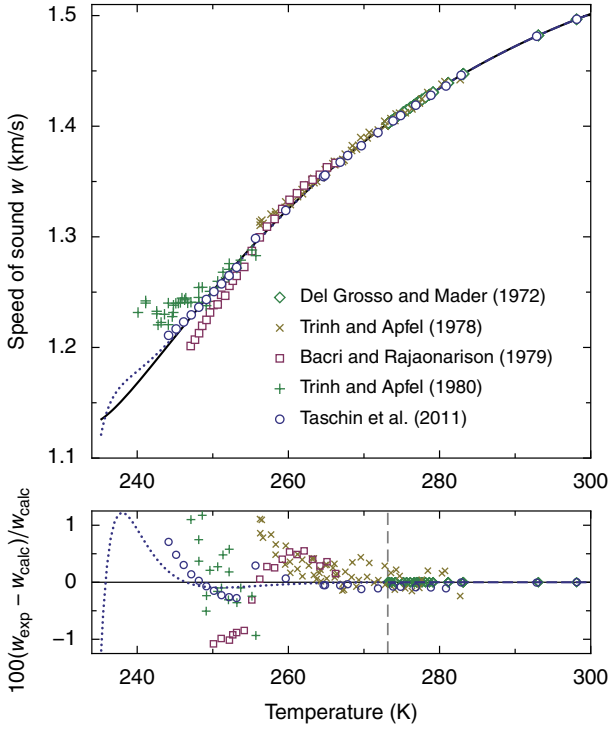

FIG. 17. Experimental data on the speed of sound[61,63–67] at 0.101325 MPa, together with from values calculated from Eq. (6) (solid curve) and IAPWS-95 (dashed in the stable-liquid region and dotted in the metastable region). The bottom two graphs show percentage deviations of experimental data from Eq. (6). The vertical dashed line indicates the melting temperature.

4.4. Speed of sound

Experimental data on the speed of sound at atmospheric pressure are shown in Fig. 17 together with values calculated from Eq. (6) and IAPWS-95. In the supercooled region, Eq. (6) represents the data of Taschin *et al.*[61] to within their uncertainty of 0.7%. In the stable region, Eq. (6) represents the speed-of-sound data of Del Grosso and Mader[63] to within their uncertainty of 0.001%.

Speed-of-sound data up to 400 MPa are compared with values calculated from Eq. (6) in Fig. 18. The proposed equation represents the data of Lin and Trusler[52] to within 0.04%. For comparison, the correlation of Lin and Trusler has deviations of up to 0.2% from their data in the temperature range considered here. The IAPWS-95 formulation was fitted to the speed-of-sound data of Petitet *et al.*,[68] which systematically deviate from the data of Lin and Trusler by up to 0.2%. This deviation is the reason for the difference between IAPWS-95 and Eq. (6) in the stable region in the range of 253 K to 263 K. Speed of sound values from the correlation of Belogol'skii *et al.*[55] differ less than 0.01% from values from Eq. (6), and the data of Aleksandrov and Larkin[56] are represented to within 0.02%.

In the metastable region from 253 K to 265 K and for pressures around 50 MPa, there is a rather large difference between the extrapolated IAPWS-95 formulation and Eq. (6) (Fig. 18). At 253 K, the difference is more than 1%. To investi-

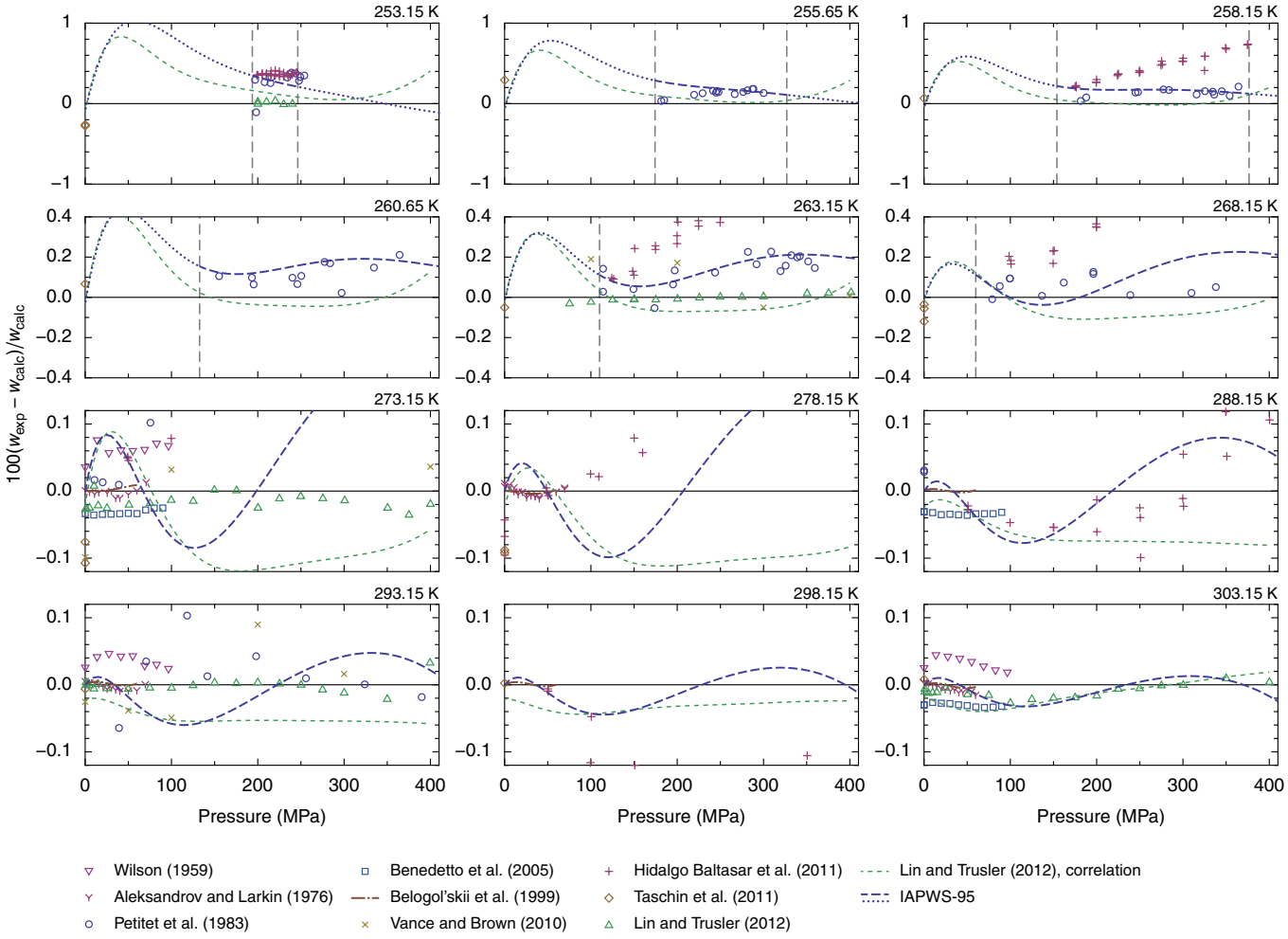

FIG. 18. Percentage deviations of experimental data on the speed of sound[52,56,59–62,68,69] from values calculated from Eq. (6). Values calculated from IAPWS-95 are plotted for comparison; dashed in the stable-liquid region and dotted in the metastable region. The correlations that Belogol'skii[55] and Lin and Trusler[52] fitted to their data are also shown. The vertical dashed lines indicate the melting pressure.

gate the nature of this difference, a test equation was forced to follow extrapolated IAPWS-95 values in the region of the difference. The density calculated from this test equation showed systematic deviations from both the data of Sotani *et al.*[35] and Asada *et al.*,[37] outside the experimental uncertainty. The difference in speed of sound between extrapolated IAPWS-95 and Eq. (6) is therefore related to the difference in density between IAPWS-95 values and the data of Sotani *et al.*[35] and Asada *et al.*[37] As can be seen in Fig. 18, the two points of Lin and Trusler[52] in the metastable region at 263 K support the behavior of Eq. (6) in this region. The correlation of Lin and Trusler behaves similarly to IAPWS-95 in the metastable region; as a result, the densities derived by Lin and Trusler from their correlation are close to the IAPWS-95 values.

4.5. Heat capacity

In Fig. 19, values for the isobaric heat capacity calculated from Eq. (6) are compared with experimental data at atmospheric pressure. There are two sets of experimental data that extend down to 236 K, that of Angell *et al.*[71] and that of Archer and Carter.[81] Both Eq. (6) and IAPWS-95 agree better with the data of Angell *et al.* than with the data of Archer and Carter. In the case of IAPWS-95, this is expected, as it was fitted to the data of Angell *et al.*[71] As described in Sec. 2.4, Eq. (6) was fitted to values computed from IAPWS-95.

The data of Bertolini *et al.*[79] agree with those of Angell *et al.* after a correction that is described in Ref. 17. The data of Tombari *et al.* suggest even larger C_P values in the supercooled region than the data of Angell *et al.* In the stable region, Eq. (6) represents the accurate data of Osborne *et al.*[76] to within 0.1%. For the isochoric heat capacity C_V, both Eq. (6) and the extrapolated IAPWS-95 formulation predict a weak temperature dependence in the supercooled region at atmospheric pressure.

Sirota *et al.*[73] measured the isobaric heat capacity at pressures up to 100 MPa in the stable region. These data are compared with Eq. (6) and with IAPWS-95 in Fig. 20. The data of Sirota *et al.* show systematic deviations from both IAPWS-95 and Eq. (6).

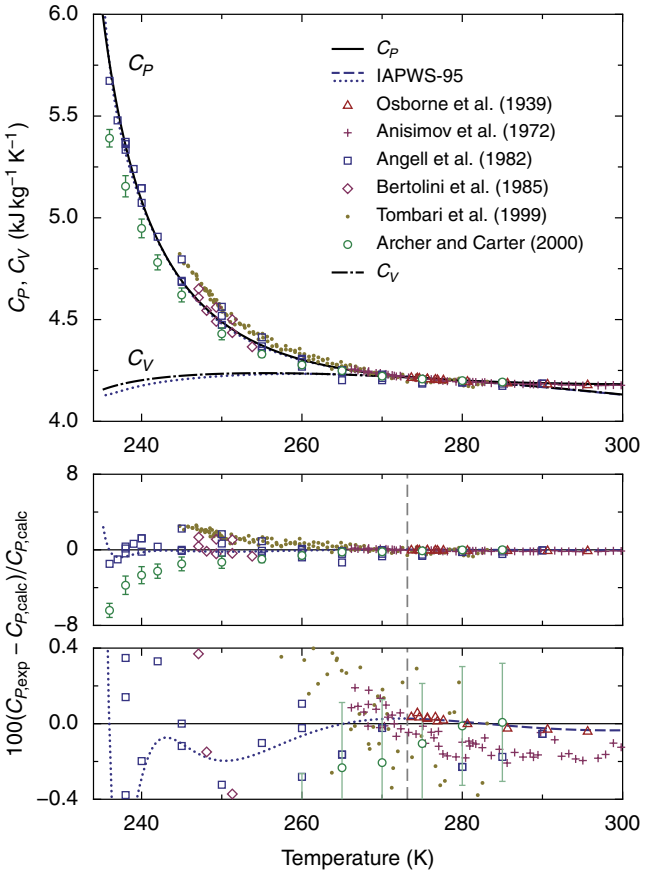

FIG. 19. Heat capacity at 0.101 325 MPa calculated from Eq. (6) (solid curve: C_P, dash-dotted curve: C_V). Symbols represent experimental data.[71,76,77,79–81] Values from IAPWS-95 are plotted for comparison; dashed in the stable-liquid region and dotted in the metastable region. The bottom two graphs show deviations of experimental C_P data from Eq. (6). The vertical dashed line indicates the melting temperature.

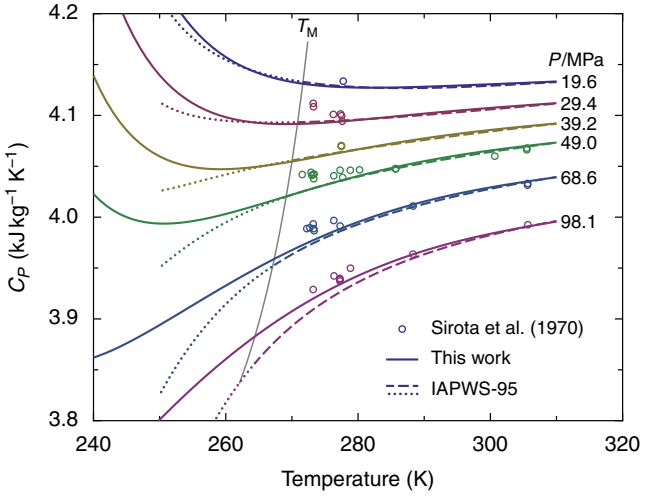

FIG. 20. Isobaric heat capacity calculated from Eq. (6) (solid curves) together with experimental data from Sirota *et al.*[73] Values from IAPWS-95 are plotted for comparison; dashed in the stable-liquid region and dotted in the metastable region. T_M denotes the melting temperature.

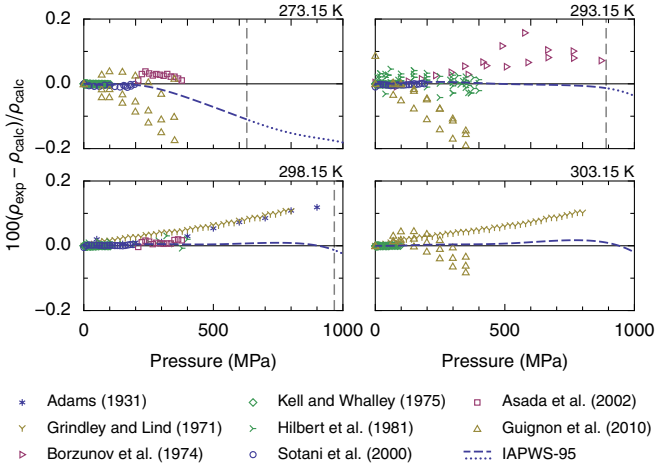

FIG. 21. Percentage deviations of experimental density data[27–30,33,35,37,39] from values calculated from Eq. (6). Values calculated from IAPWS-95 are plotted for comparison; dashed in the stable-liquid region and dotted in the metastable region. The vertical dashed lines indicate the melting pressure.

4.6. Extrapolation to 1000 MPa

There are no experimental data in the supercooled region above 400 MPa, except for one expansivity data point of Ter Minassian *et al.*[44] at 263 K and 569 MPa (Fig. 10), and two speed-of-sound measurements of Vance and Brown[59] at 263 K (up to 600 MPa, see Fig. 2). The speed-of-sound measurements of Hidalgo Baltasar *et al.*[60] in the supercooled region at 278 K and 700 MPa seem to have been affected by ice formation, because they deviate from their data in the stable-liquid region.

In the stable-liquid region below 300 K, there do exist data above 400 MPa. The expansivity data of Ter Minassian *et al.*[44] extend up to 635 MPa (Fig. 10). Grindley and Lind[28] measured densities up to 800 MPa. Figure 21 shows the deviations of experimental densities and IAPWS-95 values from Eq. (6) up to 1000 MPa. Above 293 K, Eq. (6) follows IAPWS-95 closely, while the data of Grindley and Lind[28] and Adams[27] show systematic deviations from both equations of state that increase with increasing pressure.

Both Vance and Brown[59] and Hidalgo Baltasar *et al.*[60] have measured the speed of sound up to 700 MPa. Wang *et al.*[96] determined the speed of sound at 293 K up to the melting pressure of about 900 MPa. Their data systematically deviate by about 3% from the data of Vance and Brown,[59] and will not be considered here. The differences between speed-of-sound data and Eq. (6) up to 1000 MPa are shown in Fig. 22.

The isochoric heat capacity C_P was measured by Czarnota[74] at 300 K up to 1000 MPa. Abramson and Brown[97] derived C_P values at 298 K up to 700 MPa from thermal diffusivity and thermal conductivity data. These data are compared with values calculated from Eq. (6) and IAPWS-95 in Fig. 23. Two data points of Czarnota are above the melting pressure, but Czarnota reported that the water was still liquid for those measurements.

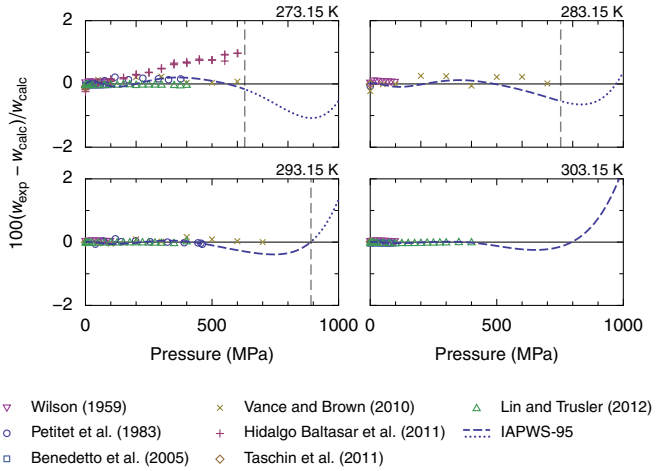

FIG. 22. Percentage deviations of experimental data on the speed of sound[52,59–62,68,69] from values calculated from Eq. (6). Values calculated from IAPWS-95 are plotted for comparison; dashed in the stable-liquid region and dotted in the metastable region. The vertical dashed lines indicate the melting pressure.

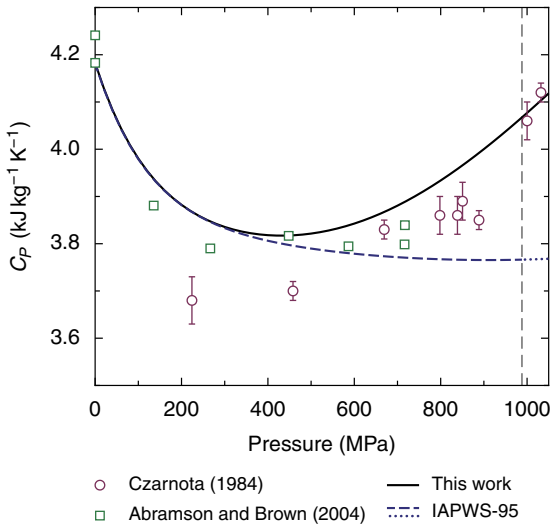

FIG. 23. Isobaric heat capacities C_P at 299.5 K calculated from Eq. (6) and IAPWS-95 (dashed in the stable-liquid region and dotted in the metastable region). Also shown are experimental data of Czarnota[74] in the range of 298.8 K to 300.1 K and data of Abramson and Brown[97] at 298.15 K, derived from thermal diffusivity and thermal conductivity measurements. The vertical dashed line indicates the melting pressure.

4.7. Connection to IAPWS-95

Because Eq. (6) was fitted to values calculated from IAPWS-95 in a part of the temperature and pressure range (see Eq. (3) and Fig. 3), the differences between the two equations of state are small in that region. Therefore, there are no large discontinuities when one switches from Eq. (6) to IAPWS-95 there. For example, one can switch from one equation to the other at the isotherm

$$T = 320\ \mathrm{K}, \tag{35}$$

TABLE V. Differences between Eq. (6) and IAPWS-95 along Eq. (35) in the P–T plane, for pressures from 0 MPa to 400 MPa

Quantity	Mean[a]	Maximum[b]
Density	0.0006%	0.0017%
Expansivity	0.010 K^{-1}	0.021 K^{-1}
Compressibility	0.02%	0.05%
Heat capacity C_P	0.02%	0.05%
Speed of sound	0.005%	0.012%

[a] Average absolute difference
[b] Maximum absolute difference

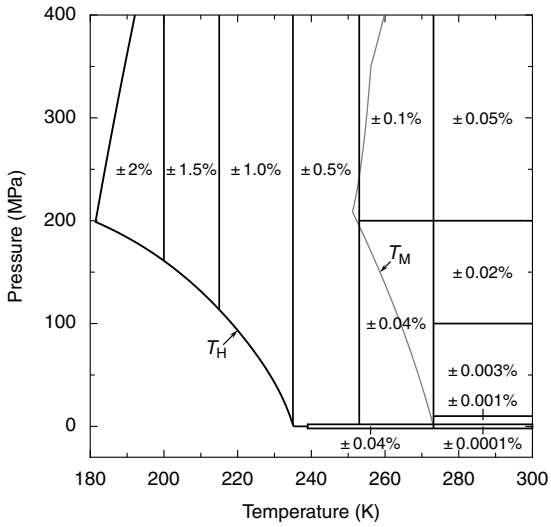

FIG. 24. Uncertainties in density estimated for Eq. (6). The thin rectangles around zero pressure refer to atmospheric pressure (0.101325 MPa). T_M indicates the melting temperature and T_H the homogeneous nucleation temperature (Appendix A). The melting curve does not separate uncertainty regions.

The differences between Eq. (6) and IAPWS-95 along this isotherm are given in Table V.

4.8. Uncertainty estimates

Uncertainty estimates for the density calculated from Eq. (6) are shown in Fig. 24. These estimates are based on the differences between Eq. (6) and experimental data, as well as on the uncertainty of the data. In a large region of the phase diagram below 253 K, only Mishima's data are available. The estimates in that region are conservative to account for the unknown systematic error of Mishima's data. Uncertainty estimates for the speed of sound calculated from Eq. (6) are shown in Fig. 25. In the region above atmospheric pressure and below 253 K, no estimates are given because of the absence of experimental data.

4.9. Ice I melting curve

As an additional test of the accuracy of the equation of state, the melting curve of ice I was calculated from the phase-

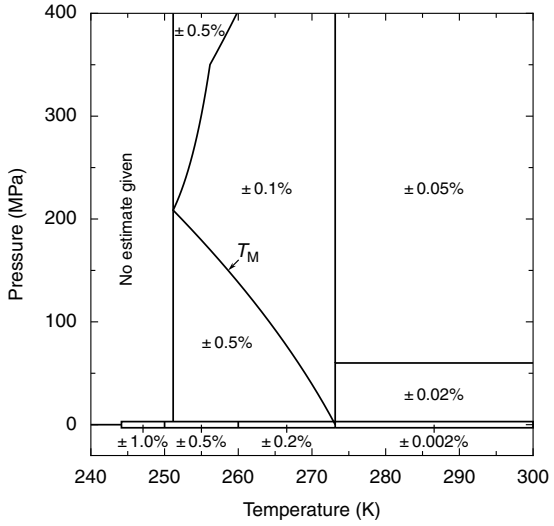

FIG. 25. Uncertainties in speed of sound estimated for Eq. (6). The thin rectangles around zero pressure refer to atmospheric pressure (0.101325 MPa). T_M indicates the melting temperature. In the region labeled "No estimate given", there are no experimental data for the speed of sound; this region extends down to the homogeneous nucleation temperature.

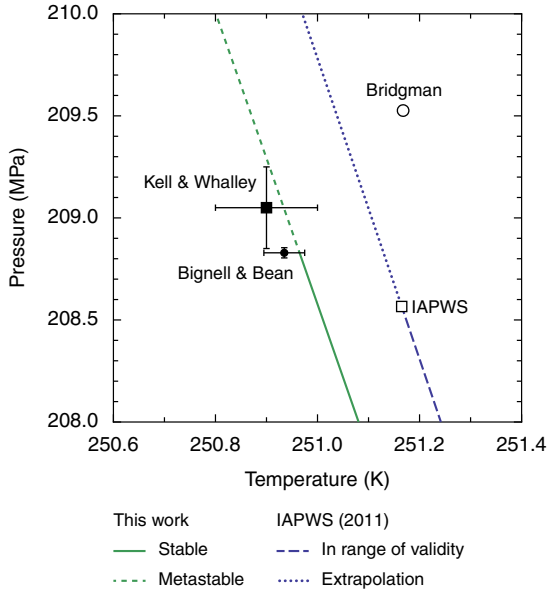

FIG. 26. Locations of the ice I–ice III–liquid triple point reported by Bridgman,[42] Kell and Whalley,[43] and Bignell and Bean.[101] The green curve is the ice I melting curve calculated from Eq. (36); solid in the stable region and dashed in the metastable region. The triple point and melting curve from IAPWS[40,41] are shown for comparison.

equilibrium condition

$$G(T,P) = G_{\mathrm{I}}(T,P). \tag{36}$$

Here, G_{I} is the Gibbs energy of ice I, which was calculated from the equation of state of Feistel and Wagner.[98] The Gibbs energy of liquid water G was calculated from Eq. (6), with zero points of entropy S and Gibbs energy chosen such that

$$S(T_{\mathrm{t}},P_{\mathrm{t}}) = 0, \tag{37}$$
$$G(T_{\mathrm{t}},P_{\mathrm{t}}) = G_{\mathrm{I}}(T_{\mathrm{t}},P_{\mathrm{t}}), \tag{38}$$

where T_{t} and P_{t} are the temperature and pressure at the ice I–liquid–vapor triple point, with[99]

$$T_{\mathrm{t}} = 273.16\ \mathrm{K}, \tag{39}$$
$$P_{\mathrm{t}} = 611.654\,771\,007\,894\ \mathrm{Pa}. \tag{40}$$

The value for the triple-point pressure given here is not the experimental value, but was calculated[99] from the IAPWS-95 formulation and the equation of state of ice I.[98] The calculated value agrees with the experimental value of (611.657 ± 0.010) Pa.[100] Equation (37) represents the convention that the specific entropy S of liquid water is zero at the triple point.[20] Equation (38) ensures that the melting curve calculated from Eq. (36) crosses the triple point.

The melting curve of ice I crosses the triple point of ice I, ice III and liquid water at about 209 MPa. Experimental locations of the I-III-L triple point are shown in Fig. 26. Bridgman[42] located the triple point in 1912. As described by Babb[102] and La Mori,[103] Bridgman's pressure values are about 1% low. For this work, Bridgman's pressures were multiplied by the correction factor 1.0102, which follows from the current value of the mercury melting pressure.[104] Kell and Whalley[43] reported the location of the triple point as part of their investigation of the ice I–ice III phase transition line. Bignell and Bean[101] determined the triple-point pressure with metrological accuracy (0.01%). Their measurements of the triple-point pressure and temperature are currently the best available. As seen in Fig. 26, the melting curve calculated from Eq. (36) agrees with the measurement of Bignell and Bean.[101]

Bridgman located 14 points on the ice I melting curve.[42]

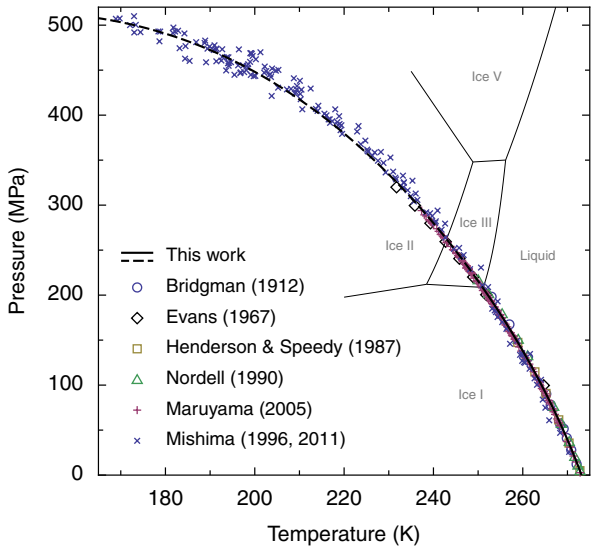

FIG. 27. Measurements of the ice I melting curve.[42,105–110] The thick curve is the predicted melting curve, calculated from Eq. (36) (solid in the stable region and dashed in the metastable region). Thin curves are the boundaries of other ices.[41–43]

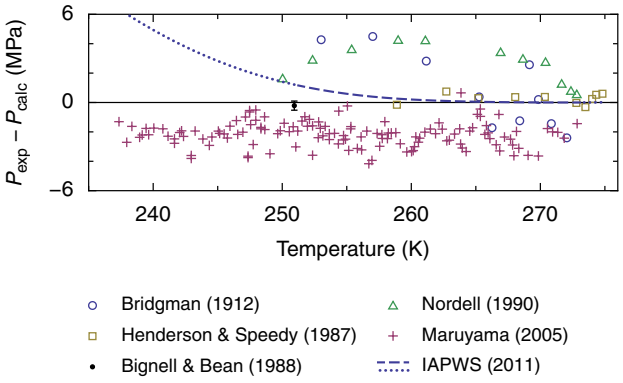

FIG. 28. Difference between experimental pressures on the ice I melting curve[42,101,106–108] and the pressure calculated from Eq. (36). The melting curve from IAPWS[40,41] is shown for comparison (dashed in the stable region and dotted in the metastable region). Note that the expression from IAPWS is valid only in the stable region; the values in the metastable region were obtained by extrapolation.

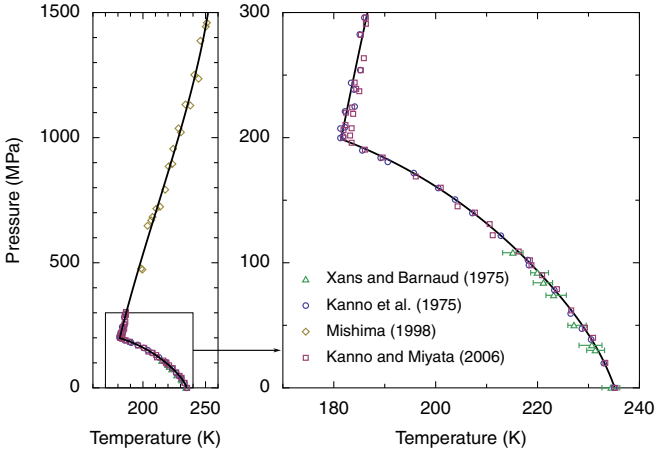

FIG. 29. Temperature of homogenous ice nucleation for micrometer-size samples. Symbols represent experimental data,[112–115] and the curve is given by Eqs. (A1) and (A2).

Of these, four points are unreliable according to Bridgman, so they will not be considered here. About 60 points on the melting curve were determined by Kishimoto and Maruyama,[111] who found a discontinuity in the melting curve at 160 MPa. In a follow-up study, Maruyama[108] did not observe the discontinuity, and suggested that it could have been an artifact of the previous experimental setup. Mishima[109,110] determined the course of the melting curve in the range where ice I is metastable. Equation (36) was used to calculate the melting curve in this range by extrapolating both the equation of state of ice and of that of supercooled water. Figure 27 shows that the calculated melting curve agrees fairly well with Mishima's data. Figure 28 shows deviations of the experimental data from values computed from Eq. (36). The data from Henderson and Speedy[106] are the most accurate and differ less than 1 MPa from Eq. (36). The data of Maruyama[108] systematically lie 2 MPa below Eq. (36). The maximum pressure difference in the stable region between Eq. (36) and values from the IAPWS correlation[41] is 0.6%, which is well within the uncertainty of 2% of the IAPWS correlation.

5. Conclusion

We have developed an equation of state for cold and supercooled water, explicit in the Gibbs energy, valid from the homogeneous nucleation temperature to 300 K and for pressures up to 400 MPa. The equation is based on a two-state model of water, combined with empirical background terms. It is the first equation of state that represents the density data of Sotani *et al.*[35] and Asada *et al.*[37] as well as the speed-of-sound data of Lin and Trusler[52] in the considered temperature range. In part of the stable region of liquid water, the equation can be connected to the IAPWS-95 formulation with minimal discontinuities in the property values.

To improve the accuracy of future equations of state, density measurements with an accuracy of 0.02% or better below 250 K up to 400 MPa are desirable. Currently, this area is only covered by Mishima's data. For the speed of sound, there are only a few measurements in the metastable region for pressures higher than atmospheric. Experimental data are needed especially down to 250 K and up to 200 MPa. Also, there are no data for the heat capacity of supercooled water above atmospheric pressure, while such data are highly desirable.

Acknowledgments

The research has been supported by the Division of Chemistry of the US National Science Foundation under Grant No. CHE-1012052. The research of V.H. was also supported by the International Association for the Properties of Water and Steam. We have benefited from discussions in the IAPWS Task Group on metastable water. A report of W. Wagner and M. Thol[49] on the behavior of IAPWS-95 has also been helpful. We thank O. Mishima for pointing out to us the existence of a minimum in the expansivity derived from the data of Grindley and Lind, and for sending us his data on the melting curves of ice. We are also grateful to M. Maruyama for making available to us his data on the ice I melting curve.

Appendix A: Homogeneous Nucleation Curve

Liquid water can be supercooled down to the homogenous ice nucleation temperature T_H, which is about 235 K at atmospheric pressure. At higher pressures, T_H is lower, with a minimum of 181 K at 200 MPa. The pressure dependence of T_H has been measured by Xans and Barnaud[112], Kanno *et al.*[113] and Kanno and Miyata[114] at pressures below 300 MPa; see Fig. 29. Mishima[115] has measured T_H at pressures from 500 MPa to 1500 MPa. At about 200 MPa, there is a break in the T_H curve as a result of nucleation of a different kind of ice above this pressure (ice III according to Kanno *et al.*[113,116] and ice II according to Kanno and Miyata[114]). For pressures below

the break point, the shape of the T_H curve can be described by an equation of the Simon type, which was also used by Wagner *et al.*[117] to describe the melting curves of water. A fit of such an equation to the data of Kanno *et al.*[113] and Kanno and Miyata[114] yields the pressure P_H on the homogeneous nucleation curve as a function of the temperature T,

$$P_H/P_0 = 1 + 2282.7(1-\theta^{6.243}) + 157.24(1-\theta^{79.81}), \quad \text{(A1)}$$

where $\theta = T/T_0$, $T_0 = 235.15$ K, and $P_0 = 0.1$ MPa. Above the break point, a third-order polynomial was fitted to the data, including Mishima's data up to 1500 MPa, which resulted in

$$\begin{aligned} T_H/\mathrm{K} =& 172.82 + 0.03718 p_1 + 3.403\times10^{-5} p_1^2 \\ & - 1.573\times10^{-8} p_1^3, \end{aligned} \quad \text{(A2)}$$

with $p_1 = P/\mathrm{MPa}$. This polynomial is based on the assumption that the T_H curve is smooth at pressures above the break point. However, because there are only few data in the range of 300 MPa to 600 MPa, the existence of other break points in the curve cannot be excluded. It must also be noted that unlike the melting curve, the homogenous nucleation curve is a kinetic limit and depends on the size and time scale of the experiment. The experimental homogeneous nucleation temperatures described in this section were obtained with samples having a diameter of several micrometers.

Appendix B: Derivatives

The derivatives of the field L, given by Eq. (13), are

$$L_{\hat{T}} = \frac{L_0 K_2}{2}\left(1 + \frac{1 - k_0 k_2 + k_1(p - k_2 t)}{K_1}\right), \quad \text{(B1)}$$

$$L_{\hat{P}} = \frac{L_0 K_2 (K + k_0 k_2 - k_1 p + k_1 k_2 t - 1)}{2 k_2 K_1}, \quad \text{(B2)}$$

$$L_{\hat{T}\hat{T}} = -\frac{2 L_0 K_2 k_0 k_1 k_2^2}{K_1^3}, \quad \text{(B3)}$$

$$L_{\hat{T}\hat{P}} = \frac{2 L_0 K_2 k_0 k_1 k_2}{K_1^3}, \quad \text{(B4)}$$

$$L_{\hat{P}\hat{P}} = -\frac{2 L_0 K_2 k_0 k_1}{K_1^3}. \quad \text{(B5)}$$

The derivatives of the Gibbs energy of the high-density structure $\hat{G}^A$, given by Eq. (30), are

$$\hat{G}^A_{\hat{T}}(\tau,\pi) = \sum_{i=1}^{n} c_i a_i \tau^{a_i - 1} \pi^{b_i} \mathrm{e}^{-d_i \pi}, \quad \text{(B6)}$$

$$\hat{G}^A_{\hat{P}}(\tau,\pi) = \sum_{i=1}^{n} c_i \tau^{a_i} \pi^{b_i - 1} (b_i - d_i \pi) \mathrm{e}^{-d_i \pi}, \quad \text{(B7)}$$

$$\hat{G}^A_{\hat{T}\hat{T}}(\tau,\pi) = \sum_{i=1}^{n} c_i a_i (a_i - 1) \tau^{a_i - 2} \pi^{b_i} \mathrm{e}^{-d_i \pi}, \quad \text{(B8)}$$

$$\hat{G}^A_{\hat{T}\hat{P}}(\tau,\pi) = \sum_{i=1}^{n} c_i a_i \tau^{a_i - 1} \pi^{b_i - 1} (b_i - d_i \pi) \mathrm{e}^{-d_i \pi}, \quad \text{(B9)}$$

$$\hat{G}^A_{\hat{P}\hat{P}}(\tau,\pi) = \sum_{i=1}^{n} c_i \tau^{a_i} \pi^{b_i - 2} [(d_i \pi - b_i)^2 - b_i] \mathrm{e}^{-d_i \pi}. \quad \text{(B10)}$$

TABLE VI. Parameter values for the equation of state

Parameter	Value	Unit	Parameter	Value
T_c	228.2	K	ω_0	0.521 226 9
P_c	0[a]	MPa	L_0	0.763 179 54
ρ_0	1 081.648 2	kg m^{-3}	k_0	0.072 158 686
R	461.523 087[b]	J kg^{-1} K^{-1}	k_1	−0.315 692 32
			k_2	5.299 260 8

[a] Mean-field value of the critical pressure. The actual location of the hypothesized critical point is uncertain. Account for critical fluctuations may increase this value by about 15 MPa. Correspondingly, the value for the critical temperature will decrease by about 2 K.[18]

[b] Equal to the ratio of the molar gas constant[118] $R_m = 8.314\,462\,1$ J mol^{-1} K^{-1} and the molar mass[20] $M = 18.015\,268$ g mol^{-1}.

TABLE VII. Parameter values for Eq. (30)

i	c_i	a_i	b_i	d_i
1	−8.157 068 138 165 5	0	0	0
2	1.287 503 2	0	1	0
3	7.090 167 359 801 2	1	0	0
4	$-3.277\,916\,1\times10^{-2}$	−0.2555	2.1051	−0.0016
5	$7.370\,394\,9\times10^{-1}$	1.5762	1.1422	0.6894
6	$-2.162\,862\,2\times10^{-1}$	1.6400	0.9510	0.0130
7	−5.178 247 9	3.6385	0	0.0002
8	$4.229\,351\,7\times10^{-4}$	−0.3828	3.6402	0.0435
9	$2.359\,210\,9\times10^{-2}$	1.6219	2.0760	0.0500
10	4.377 375 4	4.3287	−0.0016	0.0004
11	$-2.996\,777\,0\times10^{-3}$	3.4763	2.2769	0.0528
12	$-9.655\,801\,8\times10^{-1}$	5.1556	0.0008	0.0147
13	3.759 528 6	−0.3593	0.3706	0.8584
14	1.263 244 1	5.0361	−0.3975	0.9924
15	$2.854\,269\,7\times10^{-1}$	2.9786	2.9730	1.0041
16	$-8.599\,494\,7\times10^{-1}$	6.2373	−0.3180	1.0961
17	$-3.291\,615\,3\times10^{-1}$	4.0460	2.9805	1.0228
18	$9.001\,961\,6\times10^{-2}$	5.3558	2.9265	1.0303
19	$8.114\,972\,6\times10^{-2}$	9.0157	0.4456	1.6180
20	−3.278 821 3	1.2194	0.1298	0.5213

Note: the values of c_1 and c_3 do not affect measurable properties, but only the zero points of energy and entropy. The values shown here were calculated to satisfy Eqs. (37) and (38).

Appendix C: Tables

The values of the parameters that are necessary to evaluate Eq. (6) are listed in Table VI and Table VII. For the verification of computer programs, Table VIII lists calculated values for several properties. The values are given with more digits than their accuracy justifies, to enable a more detailed verification. Computer code for the equation of state is included in the supplemental material.[88]

References

[1] D. G. Fahrenheit, Phil. Trans. **33**, 78 (1724).
[2] D. Rosenfeld and W. L. Woodley, Nature **405**, 440 (2000).
[3] A. J. Heymsfield and L. M. Miloshevich, J. Atmos. Sci. **50**, 2335 (1993).
[4] J. W. P. Schmelzer and O. Hellmuth, eds., *Nucleation Theory and Applica-*

TABLE VIII. Calculated property values for computer program verification

T / K	P / MPa	ρ / kg m^{-3}	α_P / 10^{-4} K^{-1}	κ_T / 10^{-4} MPa^{-1}	C_P / J kg^{-1} K^{-1}	w / m s^{-1}	x_e	L
273.15	0.101325	999.842 29	−0.683 042	5.088 499	4 218.300 2	1 402.388 6	0.096 654 72	0.621 204 74
235.15	0.101325	968.099 99	−29.633 816	11.580 785	5 997.563 2	1 134.585 5	0.255 102 86	0.091 763 676
250	200	1 090.456 77	3.267 768	3.361 311	3 708.390 2	1 668.202 0	0.030 429 27	0.723 770 81
200	400	1 185.028 00	6.716 009	2.567 237	3 338.525	1 899.329 4	0.007 170 08	1.155 396 5
250	400	1 151.715 17	4.929 927	2.277 029	3 757.214 4	2 015.878 2	0.005 358 84	1.434 514 5

tions: Special Issues, Vol. 1 (Joint Institute for Nuclear Research, Dubna, 2013).

[5] R. Skogseth, F. Nilsen, and L. H. Smedsrud, J. Glaciology **55**, 43 (2009).

[6] T. Nash, *Cryobiology* (Academic, New York, 1966).

[7] Y. Song, R. Sharp, F. Lu, and M. Hassan, Cryobiology **60**, S60 (2010).

[8] L. Otero, A. D. Molina-García, and P. D. Sanz, Crit. Rev. Food Sci. Nutrit., **42**, 339 (2002).

[9] P. H. Poole, F. Sciortino, U. Essmann, and H. E. Stanley, Nature (London) **360**, 324 (1992).

[10] O. Mishima and H. E. Stanley, Nature **396**, 329 (1998).

[11] H. Sato, in *Properties of Water and Steam: Proceedings of the 11th International Conference*, edited by M. Píchal and O. Šifner (Hemisphere, New York, 1990) pp. 48–55.

[12] C. A. Jeffery and P. H. Austin, J. Geophys. Res. **102**, 25269 (1997).

[13] C. A. Jeffery and P. H. Austin, J. Chem. Phys. **110**, 484 (1999).

[14] S. B. Kiselev and J. F. Ely, J. Chem. Phys. **116**, 5657 (2002).

[15] D. A. Fuentevilla and M. A. Anisimov, Phys. Rev. Lett. **97**, 195702 (2006), erratum *ibid.* **98**, 149904 (2007).

[16] C. E. Bertrand and M. A. Anisimov, J. Phys. Chem. B **115**, 14099 (2011).

[17] V. Holten, C. E. Bertrand, M. A. Anisimov, and J. V. Sengers, J. Chem. Phys. **136**, 094507 (2012).

[18] V. Holten and M. A. Anisimov, Sci. Rep. **2**, 713 (2012).

[19] T. Loerting, K. Winkel, M. Seidl, M. Bauer, C. Mitterdorfer, P. H. Handle, C. G. Salzmann, E. Mayer, J. L. Finney, and D. T. Bowron, Phys. Chem. Chem. Phys. **13**, 8783 (2011).

[20] W. Wagner and A. Pruß, J. Phys. Chem. Ref. Data **31**, 387 (2002).

[21] *Revised Release on the IAPWS Formulation 1995 for the Thermodynamic Properties of Ordinary Water Substance for General and Scientific Use*, International Association for the Properties of Water and Steam (2009), available from www.iapws.org.

[22] C. A. Angell, in *Water and Aqueous Solutions at Subzero Temperatures*, Water: A Comprehensive Treatise, Vol. 7, edited by F. Franks (Plenum, New York, 1982) Chap. 1, pp. 1–81.

[23] C. A. Angell, Ann. Rev. Phys. Chem. **34**, 593 (1983).

[24] H. Sato, K. Watanabe, J. M. H. Levelt Sengers, J. S. Gallagher, P. G. Hill, J. Straub, and W. Wagner, J. Phys. Chem. Ref. Data **20**, 1023 (1991).

[25] P. G. Debenedetti, J. Phys.: Condens. Matter **15**, R1669 (2003).

[26] V. Holten, J. Kalová, M. A. Anisimov, and J. V. Sengers, Int. J. Thermophys. **33**, 758 (2012).

[27] L. H. Adams, J. Am. Chem. Soc. **53**, 3769–3813 (1931).

[28] T. Grindley and J. E. Lind, Jr., J. Chem. Phys. **54**, 3983 (1971).

[29] V. A. Borzunov, V. N. Razumikhin, and V. A. Stekol'nikov, in *Thermophysical properties of matter and substances*, Vol. 2, edited by V. A. Rabinovich (Amerind Publishing Co., New Delhi, 1974) pp. 187–195.

[30] G. S. Kell and E. Whalley, J. Chem. Phys. **62**, 3496 (1975).

[31] A. Bradshaw and K. Schleicher, Deep-Sea Res. **23**, 583 (1976).

[32] A. A. Aleksandrov, T. S. Khasanshin, and D. K. Larkin, Zh. Fiz. Khim. **50**, 394 (1976); Russ. J. Phys. Chem. **50**, 231 (1976).

[33] R. Hilbert, K. Tödheide, and E. U. Franck, Ber. Bunsenges. Phys. Chem. **85**, 636 (1981).

[34] D. E. Hare and C. M. Sorensen, J. Chem. Phys. **87**, 4840 (1987).

[35] T. Sotani, J. Arabas, H. Kubota, and M. Kijima, High Temp.-High Press. **32**, 433 (2000).

[36] M. Tanaka, G. Girard, R. Davis, A. Peuto, and N. Bignell, Metrologia **38**, 301 (2001).

[37] S. Asada, T. Sotani, J. Arabas, H. Kubota, S. Matsuo, and Y. Tanaka, J. Phys.: Condens. Matter **14**, 11447 (2002).

[38] O. Mishima, J. Chem. Phys. **133**, 144503 (2010).

[39] B. Guignon, C. Aparicio, and P. D. Sanz, J. Chem. Eng. Data **55**, 3338 (2010).

[40] *Revised Release on the Pressure along the Melting and Sublimation Curves of Ordinary Water Substance*, International Association for the Properties of Water and Steam (2011), available from www.iapws.org.

[41] W. Wagner, T. Riethmann, R. Feistel, and A. H. Harvey, J. Phys. Chem. Ref. Data **40**, 043103 (2011).

[42] P. W. Bridgman, Proc. Am. Acad. Arts Sci. **47**, 441 (1912).

[43] G. S. Kell and E. Whalley, J. Chem. Phys. **48**, 2359 (1968).

[44] L. Ter Minassian, P. Pruzan, and A. Soulard, J. Chem. Phys. **75**, 3064 (1981).

[45] D. R. Caldwell, Deep-Sea Res. **25**, 175 (1978).

[46] R. J. Speedy and C. A. Angell, J. Chem. Phys. **65**, 851 (1976).

[47] H. Kanno and C. A. Angell, J. Chem. Phys. **70**, 4008 (1979).

[48] T. Sotani, H. Kubota, and A. Sakata, High Temp.-High Press. **30**, 509 (1998).

[49] W. Wagner and M. Thol, "The behavior of IAPWS-95 at temperatures from 250 K to 300 K and pressures up to 400 MPa," Report prepared for the Task Group Subcooled Water and the Working Group Thermophysical Properties of Water and Steam, International Association for the Properties of Water and Steam (Chair of Thermodynamics, Ruhr-University Bochum, Germany, 2013).

[50] V. Tekáč, I. Cibulka, and R. Holub, Fluid Phase Equilib. **19**, 33 (1985).

[51] T. W. Kazuki Hiro and S. Kumagai, Phys. Chem. Liq. (2013), 10.1080/00319104.2013.793598.

[52] C.-W. Lin and J. P. M. Trusler, J. Chem. Phys. **136**, 094511 (2012).

[53] A. H. Smith and A. W. Lawson, J. Chem. Phys. **22**, 351 (1954).

[54] G. Holton, M. P. Hagelberg, S. Kao, and W. H. Johnson, Jr., J. Acoust. Soc. Am. **43**, 102 (1968).

[55] V. A. Belogol'skii, S. S. Sekoyan, L. M. Samorukova, S. R. Stefanov, and V. I. Levtsov, Meas. Tech. **42**, 406 (1999); See also: C. C. Leroy, S. P. Robinson, and M. J. Goldsmith, J. Acoust. Soc. Am. **124**, 2774 (2008).

[56] A. A. Aleksandrov and D. K. Larkin, Thermal Eng. **23**, 72 (1976); Teploenergetika **23**, 75 (1976).

[57] A. M. Mamedov, J. Eng. Phys. **36**, 113 (1979); Inzh. Fiz. Zh. **36**, 156 (1979).

[58] A. A. Aleksandrov and A. I. Kochetov, Thermal Eng. **26**, 558 (1979); Teploenergetika **26**, 65 (1979).

[59] S. Vance and J. M. Brown, J. Acoust. Soc. Am. **127**, 174 (2010).

[60] E. Hidalgo Baltasar, M. Taravillo, V. G. Baonza, P. D. Sanz, and B. Guignon, J. Chem. Eng. Data **56**, 4800 (2011).

[61] A. Taschin, R. Cucini, P. Bartolini, and R. Torre, Phil. Mag. **91**, 1796 (2011).

[62] W. D. Wilson, J. Acoust. Soc. Am. **31**, 1067 (1959).

[63] V. A. Del Grosso and C. W. Mader, J. Acoust. Soc. Am. **52**, 1442 (1972).

[64] E. Trinh and R. E. Apfel, J. Acoust. Soc. Am. **63**, 777 (1978).

[65] E. Trinh and R. E. Apfel, J. Chem. Phys. **69**, 4245 (1978).

[66] J.-C. Bacri and R. Rajaonarison, J. Physique Lett. **40**, L403 (1979).

[67] E. Trinh and R. E. Apfel, J. Chem. Phys. **72**, 6731 (1980).

[68] J. P. Petitet, R. Tufeu, and B. Le Neindre, Int. J. Thermophys. **4**, 35 (1983).

[69] G. Benedetto, R. M. Gavioso, P. A. Giuliano Albo, S. Lago, D. Madonna Ripa, and R. Spagnolo, Int. J. Thermophys. **26**, 1667 (2005).

[70] A. Taschin, P. Bartolini, R. Eramo, and R. Torre, Phys. Rev. E **74**, 031502 (2006).

[71] C. A. Angell, M. Oguni, and W. J. Sichina, J. Phys. Chem. **86**, 998 (1982).

[72] D. G. Archer, J. Phys. Chem. Ref. Data **22**, 1441 (1993).

[73] A. M. Sirota, A. Ya. Grishkov, and A. G. Tomishko, Thermal Eng. **17**, 90 (1970).
[74] I. Czarnota, High Temp.-High Press. **16**, 295 (1984).
[75] J. J. Manyà, M. J. Antal, Jr., C. K. Kinoshita, and S. M. Masutani, Ind. Eng. Chem. Res. **50**, 6470 (2011).
[76] N. S. Osborne, H. F. Stimson, and D. C. Ginnings, J. Res. Natl. Bur. Stand. **23**, 197 (1939).
[77] M. A. Anisimov, A. V. Voronel', N. S. Zaugol'nikova, and G. I. Ovodov, JETP Lett. **15**, 317 (1972).
[78] C. A. Angell, J. Shuppert, and J. C. Tucker, J. Phys. Chem. **77**, 3092 (1973).
[79] D. Bertolini, M. Cassettari, and G. Salvetti, Chem. Phys. Lett. **199**, 553 (1985).
[80] E. Tombari, C. Ferrari, and G. Salvetti, Chem. Phys. Lett. **300**, 749 (1999).
[81] D. G. Archer and R. W. Carter, J. Phys. Chem. B **104**, 8563 (2000).
[82] H. Preston-Thomas, Metrologia **27**, 3 (1990).
[83] R. L. Rusby, J. Chem. Thermodyn. **23**, 1153 (1991).
[84] R. E. Bedford and C. G. M. Kirby, Metrologia **5**, 83 (1969).
[85] T. B. Douglas, J. Res. Nat. Bur. Stand. **73A**, 451 (1969).
[86] R. N. Goldberg and R. D. Weir, Pure Appl. Chem. **64**, 1545 (1992).
[87] R. D. Weir and R. N. Goldberg, J. Chem. Thermodyn. **28**, 261 (1996).
[88] See "Ancillary files" links on the arXiv article page for tables with experimental data and computer code for the equation of state.
[89] A. Nilsson, C. Huang, and L. G. Pettersson, J. Mol. Liq. **176**, 2 (2012).
[90] A. Taschin, P. Bartolini, R. Eramo, R. Righini, and R. Torre, Nat. Commun. **4**, 2401 (2013).
[91] O. Mishima, Phys. Rev. Lett. **85**, 334 (2000).
[92] V. Holten and M. A. Anisimov, Sci. Rep. **2**, 713 (2012), supplementary information.
[93] E. W. Lemmon, M. O. McLinden, and W. Wagner, J. Chem. Eng. Data **54**, 3141 (2009).
[94] S. J. Henderson and R. J. Speedy, J. Phys. Chem. **91**, 3062 (1987).
[95] F. J. Millero, R. W. Curry, and W. Drost-Hansen, J. Chem. Eng. Data **14**, 422 (1969).
[96] Z.-G. Wang, Y.-G. Liu, W.-G. Zhou, W. Song, Y. Bi, L. Liu, and H.-S. Xie, Chin. Phys. Lett. **30**, 054302 (2013).
[97] E. H. Abramson and J. M. Brown, Geochim. Cosmochim. Acta **68**, 1827 (2004).
[98] R. Feistel and W. Wagner, J. Phys. Chem. Ref. Data **35**, 1021 (2006).
[99] R. Feistel, D. G. Wright, K. Miyagawa, A. H. Harvey, J. Hruby, D. R. Jackett, T. J. McDougall, and W. Wagner, Ocean Sci. **4**, 275 (2008).
[100] L. A. Guildner, D. P. Johnson, and F. E. Jones, J. Res. Natl. Bur. Stand. **80A**, 505 (1976).
[101] N. Bignell and V. E. Bean, Metrologia **25**, 205 (1988).
[102] S. E. Babb, Jr., in *High-Pressure Measurement*, edited by A. A. Giardini and E. C. Lloyd (Butterworths, Washington, 1963) pp. 115–124.
[103] P. N. La Mori, in *1964 Symposium on High-Pressure Technology*, edited by E. C. Lloyd and A. A. Giardini (American Society of Mechanical Engineers, New York, 1965) paper 64-WA/PT-25.
[104] G. F. Molinar, V. Bean, J. Houck, and B. Welch, Metrologia **16**, 21 (1980).
[105] L. F. Evans, J. Appl. Phys. **38**, 4930 (1967).
[106] S. J. Henderson and R. J. Speedy, J. Phys. Chem. **91**, 3069 (1987).
[107] B. Nordell, Cold Reg. Sci. Technol. **19**, 83 (1990).
[108] M. Maruyama, J. Crystal Growth **275**, 598 (2005).
[109] O. Mishima, Nature **384**, 546 (1996).
[110] O. Mishima, J. Phys. Chem. B **115**, 14064 (2011).
[111] Y. Kishimoto and M. Maruyama, Rev. High Pressure Sci. Technol. **7**, 1144 (1998).
[112] P. Xans and G. Barnaud, C. R. Acad. Sci. Paris **280**, 25 (1975).
[113] H. Kanno, R. J. Speedy, and C. A. Angell, Science **189**, 880 (1975).
[114] H. Kanno and K. Miyata, Chem. Phys. Lett. **422**, 507 (2006).
[115] O. Mishima and H. E. Stanley, Nature **392**, 164 (1998).
[116] H. Kanno and C. A. Angell, J. Phys. Chem. **81**, 2639 (1977).
[117] W. Wagner, A. Saul, and A. Pruß, J. Phys. Chem. Ref. Data **23**, 515 (1994).
[118] P. J. Mohr, B. N. Taylor, and D. B. Newell, Rev. Mod. Phys. **84**, 1527 (2012).